Available online at www.sciencedirect.com
ScienceDirect
Journal of Computational Physics 222 (2007) 217–245
JOURNAL OF COMPUTATIONAL PHYSICS
www.elsevier.com/locate/jcp

An exact Riemann solver for compressible two-phase flow models containing non-conservative products

Vincent Deledicque, Miltiadis V. Papalexandris *

Département de Mécanique, Université Catholique de Louvain, Place du Levant 2, 1348 Louvain-la-Neuve, Belgium

Received 28 March 2006; received in revised form 23 June 2006; accepted 20 July 2006
Available online 12 September 2006

Abstract

In this article we present a new numerical procedure for solving exactly the Riemann problem of compressible two-phase flow models containing non-conservative products. These products appear in the expressions for the interactions between the two phases. Thus, in the compressible limit, the governing equations are hyperbolic but can not be written as conservation laws, *i.e.* in divergence form. In general, the solution to the Riemann problem of these models contains six distinct centered waves. According to the relative position of these waves in the x–t plane, the possible solutions can be classified into four principal configurations. The Riemann solver we propose herein investigates sequentially each of these configurations until an admissible solution is calculated. Special configurations, corresponding to coalescence of waves, are also analyzed and included in the solver. Further, we examine the accuracy and robustness of three known methods for the integration of the non-conservative products, via a series of numerical tests. Finally, the issue of existence and uniqueness of solutions to the Riemann problem is discussed.

Keywords: Two-phase flows; Shocks; Riemann solver; Non-conservative products; Nozzling terms

1. Introduction

In this article we derive a numerical procedure for solving exactly the Riemann problem associated to compressible two-phase flow models that contain non-conservative products. Such flows arise in various natural phenomena and technological applications, such as sandstorms, volcanic eruptions, power plants, chemical plants, solid rocket motors, deflagration-to-detonation transition in granular explosives, and others. These flows are quite hard to study because of the existence of a multitude of spatial and temporal scales and because of the complexity of the interactions between the two phases. Nevertheless, their wide applicability has stimulated, over the years, large efforts for their better understanding. In particular, the modelling and numerical treatment of these flows have been the subject of extensive and intense research.

* Corresponding author. Tel.: +32 10 478883; fax: +32 10 452692.
E-mail address: miltos@term.ucl.ac.be (M.V. Papalexandris).

0021-9991/$ - see front matter
doi:10.1016/j.jcp.2006.07.025

Typically, two-phase models are derived by either an averaging (kinetic based) approach or a mixture-theory approach. In the averaging approach one considers that one phase consists of an ensemble of particles embedded in a carrier fluid medium. The particles can interact with each other in a prescribed way (*e.g.* collisions, coalescences, *etc.*). The number density of particles in an appropriate phase space, (*e.g.* coordinate-velocity space) is the distribution function and obeys a Boltzmann-type equation. This equation can be integrated over the phase space to yield the balance equations for the medium, Drew and Passman [1], Enwald et al. [2]. This procedure, referred to as ensemble averaging, can be replaced by time or volume averaging provided that the ergodic hypothesis is satisfied.

On the other hand, mixture theories treat the mixture as a multicomponent fluid. In other words, the mixture is assumed to consist of two separate, identifiable and co-existing continua that are in thermodynamic non-equilibrium with each other. The balance equations of each phase are derived by heuristic approaches or, more appropriately, by exploiting the entropy inequality of the mixture. Examples of mixture-theory models for compressible two-phase flows are the BN model of Baer and Nunziato [3], as well as those of Powers et al. [4], Saurel and Abgrall [5], Bdzil et al. [6] and Papalexandris [7], *etc*.

Most of the two-phase models contain non-conservative products, that is, terms with spatial derivatives that can not be written in divergence form. These terms are part of the expressions that describe momentum and energy transfer between the two phases. In the literature of two-phase flows, they are often referred to as *nozzling terms* by analogy to similar terms that appear in the equations of 1D flow in variable-area duct. In some modelling and numerical studies these terms have been ignored either by choice, Gonthier and Powers [8], or by convenience, Papalexandris [9]. However, these terms are required to guarantee that the entropy inequality is satisfied. For this reason, it is generally accepted that the nozzling terms should be included in the balance equations of the two-phase mixture.

The presence of these terms introduces serious analytical and computational difficulties. In particular, these terms do not permit the balance equations to be written in conservative (divergence) form in the hyperbolic limit. (That is, in the limit where viscosity and other dissipative terms are zero.) As a result, weak solutions of these equations can not be defined in the standard sense of distributions. In particular, jump, Rankine–Hugoniot, relations across discontinuities can not be defined in an unambiguous manner. Although there has been recent progress in the mathematical analysis of non-conservative hyperbolic equations (see, *e.g.* Dal Maso et al. [10], Lefloch and Tzavaras [11] and Crasta and Lefloch [12]), an existential theory for such equations is not yet available. More important, it has been demonstrated that due to the non-conservative products, the balance equations admit more than an unique solution under certain flow conditions, Andrianov and Warnecke [13] and Andrianov [29].

Because of these serious analytical difficulties, the derivation of efficient algorithms for the numerical treatment of the balance equations becomes a very challenging task. Additionally, since the non-conservative products do not represent fluxes, they have to be integrated as source terms. Numerical evidence has shown that there can be numerical instabilities and spurious oscillations from the integration of these terms, even when the balance equations admit a unique solution [13].

Nevertheless, non-conservative, compressible, two-phase flow models share an important property that facilitates their analysis: the balance equations of the mixture are in fact conservative. As shown by Embid and Baer [14], this implies that Rankine–Hugoniot relations can always be defined provided that a gaseous shock does not move at the solid phase speed. As will be shown later, the last condition can occur only when the gaseous shock coincides with a solid contact discontinuity, which is a very special case. In addition to this, the authors in [14] derived the Riemann invariants and constructed simple wave solutions of the BN model. It is worth mentioning that although the analysis in [14] was made for the BN model, the results hold for a broader class of two-phase flow models, *e.g.* [3,5–7], as the homogeneous part of all these models is the same.

Recently, there has also been progress in the construction of numerical methods for the flow models of interest. For example, Saurel and Abgrall [5], Saurel and Lemetayer [15] and Gavrilyuk and Saurel [16] presented numerical approximations of the nozzling terms based on a condition of Abgrall [17]. This condition states that a two-phase flow with initially uniform velocity and pressure should remain as such for all times.

On the other hand, a large number of numerical methods for hyperbolic conservation laws employ an exact or approximate solution of the local Riemann problem at the cell interfaces in order to advance the solution in time. All these algorithms belong to the family of Godunov-based methods and the literature on this subject is

vast. Applying these popular numerical methods to two-phase flows requires the design of an efficient and robust Riemann solver for the non-conservative governing system. It also requires the development of an accurate method for the integration of the non-conservative products.

A step toward this direction was made by Andrianov and Warnecke [13] who studied the inverse Riemann problem and provided solutions to it by employing the results of [14]. In a very recent paper, Schwendeman et al. [18] provided the first exact Riemann solver of the flow models of interest and a numerical procedure for the integration of non-conservative products. This solver is a two-stage method. In the first stage it is assumed that there is no initial jump in the volume fractions of the two phases. The pressures in the intermediate states are then calculated via two independent Newton iterations. The second stage takes into account the jump in the volume fractions and employs an additional Newton iteration to determine the intermediate states.

In this article we propose a different procedure for obtaining numerical solutions to the Riemann problem of interest. In particular, the algorithm proposed herein is based on grouping the possible solutions into four principal configurations, according to the relative ordering of the centered waves that are generated as the initial conditions evolve. The admissibility of each configuration is examined sequentially, and the intermediate states are calculated via two secant iterations. Special configurations, corresponding to coalescence of waves, are also analyzed and included in the solver.

In this article we also compare the efficiency of three known methods for the integration of the non-conservative products through a series of numerical tests. In these comparisons we used the classical Godunov scheme with the Riemann solver proposed herein. The most efficient of these three methods is extended to second-order accuracy and implemented in a MUSCL-type scheme.

Finally, we discuss briefly the issue of ill-posedness of the Riemann problem. As it turns out, under certain initial conditions, there is more than one entropy satisfying solution. Furthermore, there are initial conditions for which the Riemann problem does not admit any solution at all. As it turns out, such initial conditions can be obtained by slightly perturbing initial data for which solutions do exist, which indicates a severe breakdown of the validity of the two-phase flow model.

This article is organized as follows: in Section 2, we summarize the results of the characteristic analysis of [14]. In Section 3, we present the various possible wave configurations to the Riemann problem. The description of the proposed solver is given in Section 4. A brief description of available methods for the numerical integration of the non-conservative products is given in Section 5. Numerical results obtained by these methods are presented and compared in Section 6. Finally, in Section 7 we discuss the issue of ill-posedness of the Riemann problem.

2. Presentation of the governing equations and their characteristic analysis

As mentioned in Section 1, the homogeneous part of many compressible two-phase flow models, namely [3,5–7], is the same. This article focuses precisely on the Riemann problem associated to this common system of homogeneous equations. In this section, and in order to facilitate the presentation of the proposed Riemann solver, we present the set of homogeneous system of interest and summarize the results of its characteristic analysis presented in [14]. In this set of equations there is no characteristic length scale and, therefore, the solution to the Riemann problem is self-similar, *i.e.* the speeds of centered waves are constant.

It should be mentioned that the various available two-phase flow models have different algebraic source terms that describe phase interactions. This implies that, in principle, one should consider the Riemann problem for a full model (including source terms), and not just its homogeneous part. The full, non-homogeneous Riemann problem is no longer self similar, since the source terms introduce characteristic length scales. In other words, the waves that form the solution to the Riemann problem do not have constant speeds anymore. Therefore, the non-homogeneous Riemann problems of the various models are different to each other.

However, for numerical purposes it suffices to consider the (common) homogeneous Riemann problem provided that at small times the solution of the full, non-homogeneous problem converges to the solution of the homogeneous one. Although there are heuristic arguments that can be used to justify such a hypothesis for certain flow conditions, the convergence of the non-homogeneous Riemann problem to the homogeneous one, as time goes to zero, has not been proven yet.

The models under consideration treat each phase as two separate and co-existing continua. Herein, for the sake of simplicity in notation we will refer to the carrier phase as the *gaseous* phase and to the particulate one as the *solid* phase, although the models of interest can also be applied to mixtures Riemann problem to a homogeneous one as consisting of liquid particles in a gas, or gaseous bubbles in a liquid.

Each phase is assigned a density ρ_α, pressure p_α, specific internal energy e_α, velocity u_α and a volume fraction ϕ_α, where $\alpha = \mathrm{g}, \mathrm{s}$, and g and s denote the carrier "gaseous" phase and the particulate "solid" phase, respectively. The volume fractions represent the percentages of volume occupied by the constituents. Also, let T_α, η_α, $h_\alpha = e_\alpha + p_\alpha/\rho_\alpha$ and $E_\alpha = e_\alpha + \frac{u_\alpha^2}{2}$, denote the temperature, specific entropy, specific enthalpy and total specific energy for each phase, respectively.

The governing equations consist of the mass, momentum and energy balance laws for each phase plus a convection equation for the solid volume fraction,

$$\frac{\partial \phi_\mathrm{s}\rho_\mathrm{s}}{\partial t} + \frac{\partial \phi_\mathrm{s}\rho_\mathrm{s}u_\mathrm{s}}{\partial x} = 0, \tag{1a}$$

$$\frac{\partial \phi_\mathrm{s}\rho_\mathrm{s}u_\mathrm{s}}{\partial t} + \frac{\partial (\phi_\mathrm{s}\rho_\mathrm{s}u_\mathrm{s}^2 + \phi_\mathrm{s}p_\mathrm{s})}{\partial x} = p_\mathrm{g}\frac{\partial \phi_\mathrm{s}}{\partial x}, \tag{1b}$$

$$\frac{\partial \phi_\mathrm{s}\rho_\mathrm{s}E_\mathrm{s}}{\partial t} + \frac{\partial (\phi_\mathrm{s}u_\mathrm{s}(\rho_\mathrm{s}E_\mathrm{s} + p_\mathrm{s})}{\partial x} = p_\mathrm{g}u_\mathrm{s}\frac{\partial \phi_\mathrm{s}}{\partial x}, \tag{1c}$$

$$\frac{\partial \phi_\mathrm{g}\rho_\mathrm{g}}{\partial t} + \frac{\partial \phi_\mathrm{g}\rho_\mathrm{g}u_\mathrm{g}}{\partial x} = 0, \tag{1d}$$

$$\frac{\partial \phi_\mathrm{g}\rho_\mathrm{g}u_\mathrm{g}}{\partial t} + \frac{\partial (\phi_\mathrm{g}\rho_\mathrm{g}u_\mathrm{g}^2 + \phi_\mathrm{g}p_\mathrm{g})}{\partial x} = -p_\mathrm{g}\frac{\partial \phi_\mathrm{s}}{\partial x}, \tag{1e}$$

$$\frac{\partial \phi_\mathrm{g}\rho_\mathrm{g}E_\mathrm{g}}{\partial t} + \frac{\partial (\phi_\mathrm{g}u_\mathrm{g}(\rho_\mathrm{g}E_\mathrm{g} + p_\mathrm{g})}{\partial x} = -p_\mathrm{g}u_\mathrm{s}\frac{\partial \phi_\mathrm{s}}{\partial x}, \tag{1f}$$

$$\frac{\partial \phi_\mathrm{s}}{\partial t} + u_\mathrm{s}\frac{\partial \phi_\mathrm{s}}{\partial x} = 0. \tag{1g}$$

It is also assumed that the following saturation condition holds:

$$\phi_\mathrm{g} + \phi_\mathrm{s} = 1. \tag{2}$$

The above system is closed with the equations of state for each phase. It is assumed herein that the state equations are convex. Embid and Baer [14] performed a detailed characteristic analysis of the present model, a necessary task for the resolution of the Riemann problem. We rewrite here the most important results that they obtained. These results are independent of the equations of state.

The eigenvalues of the system are

$$\lambda_\mathrm{s}^- = u_\mathrm{s} - c_\mathrm{s}, \quad \lambda_\mathrm{s}^0 = u_\mathrm{s}, \quad \lambda_\mathrm{s}^+ = u_\mathrm{s} + c_\mathrm{s}, \tag{3a}$$

and

$$\lambda_\mathrm{g}^- = u_\mathrm{g} - c_\mathrm{g}, \quad \lambda_\mathrm{g}^0 = u_\mathrm{g}, \quad \lambda_\mathrm{g}^+ = u_\mathrm{g} + c_\mathrm{g}, \tag{3b}$$

where c_s, c_g denote the sound speed of the solid and gaseous phases, respectively.

The system under consideration is not strictly hyperbolic because λ_s^0 is a double eigenvalue and because certain eigenvalues can coalesce. The fields associated with λ_s^-, λ_s^+, λ_g^- and λ_g^+, are genuinely non-linear, whereas the fields associated with λ_s^0 and λ_g^0, are linearly degenerate. These linearly degenerate fields are the solid and gaseous contact discontinuities and they propagate at speeds equal to λ_s^0 and λ_g^0, respectively. The eigenvectors of the system form a basis of $\mathscr{R}^7$ except when $u_\mathrm{g} \pm c_\mathrm{g} = u_\mathrm{s}$ (choked flow). The system is therefore completely hyperbolic except in choked flow conditions.

The Riemann problem of the above system admits rarefactions, contact discontinuities and shock waves. Across rarefactions and contact discontinuities certain quantities (Riemann invariants) are conserved.

Riemann invariants across a gaseous rarefaction:

$$\psi^{\pm}_{g1} = \eta_g, \tag{4a}$$

$$\psi^{\pm}_{g2} = u_g \mp \int \rho_g^{-1} c_g \, d\rho_g, \tag{4b}$$

$$\psi^{\pm}_{g3} = \phi_g, \tag{4c}$$

$$\psi^{\pm}_{g4} = \rho_s, \tag{4d}$$

$$\psi^{\pm}_{g5} = u_s, \tag{4e}$$

$$\psi^{\pm}_{g6} = \eta_s, \tag{4f}$$

Riemann invariants across a solid rarefaction:

$$\psi^{\pm}_{s1} = \eta_s, \tag{5a}$$

$$\psi^{\pm}_{s2} = u_s \mp \int \rho_s^{-1} c_s \, d\rho_s, \tag{5b}$$

$$\psi^{\pm}_{s3} = \phi_s, \tag{5c}$$

$$\psi^{\pm}_{s4} = \rho_g, \tag{5d}$$

$$\psi^{\pm}_{s5} = u_g, \tag{5e}$$

$$\psi^{\pm}_{s6} = \eta_g. \tag{5f}$$

It is useful to note that the volume fractions are conserved across rarefactions, *cf*. (4c) and (5c). Furthermore, the above equations imply that the state of one phase remains constant across the rarefaction of the other phase. In other words (4d) and (4f) imply that the solid pressure, temperature, and internal energy are constant across a gaseous rarefaction, and *vice versa*.

It is also interesting to mention that for some simple equations of state, notably for a perfect gas, the above Riemann invariants take the form of simple algebraic expressions that can be easily used for numerical purposes. However, for complex equations of state (*e.g.* Tait equation), the computation of the Riemann invariants, especially (4b) and (5b), requires some iterative procedure.

The invariants across contact discontinuities are:

Riemann invariants across a gaseous contact discontinuity:

$$\psi^{0}_{g1} = u_g, \tag{6a}$$

$$\psi^{0}_{g2} = p_g, \tag{6b}$$

$$\psi^{0}_{g3} = \phi_s, \tag{6c}$$

$$\psi^{0}_{g4} = \rho_s, \tag{6d}$$

$$\psi^{0}_{g5} = u_s, \tag{6e}$$

$$\psi^{0}_{g6} = \eta_s. \tag{6f}$$

Riemann invariants across a solid contact discontinuity:

$$\psi^{0}_{s1} = u_s, \tag{7a}$$

$$\psi^{0}_{s2} = \eta_g, \tag{7b}$$

$$\psi^{0}_{s3} = \phi_g \rho_g (u_s - u_g), \tag{7c}$$

$$\psi^{0}_{s4} = \phi_s p_s + \phi_g p_g + \phi_g \rho_g (u_s - u_g)^2, \tag{7d}$$

$$\psi^{0}_{s5} = \frac{(u_s - u_g)^2}{2} + h_g. \tag{7e}$$

It is clear from Eq. (6) that the solid phase variables remain constant across gaseous contact lines, as was the case for gaseous rarefactions. On the contrary, Eq. (7) imply that the gaseous state does not remain constant across a solid contact line. However, the mass, momentum and energy of the mixture are conserved across a solid contact discontinuity, *cf.* (7c)–(7e), respectively.

It is also interesting to note that, by virtue of the invariant ψ^0_{s3}, if $u_s > u_g$ on one side of the solid contact discontinuity, then necessarily $u_s > u_g$ on the other side also. That means that the gas flow relative to the solid phase (and hence relative to the solid contact discontinuity) is in the same direction on both sides of the discontinuity, thus avoiding mass accumulation on the discontinuity.

As far as numerical procedures are concerned, we remark that the invariants across a gaseous contact line are trivial to compute. However, the computation of (7) may present some difficulties. In fact, the system (7) may admit zero, one or two solutions. This implies that, given the flow variables on one side of the contact line, we might not be able to unambiguously compute the flow variables on the other side.

For the sake of argument, let us suppose that the gaseous phase is a perfect gas and let γ_g denote the constant ratio of its specific heats. Further, let the subscript "L" refer to the left state and the subscript "R" refer to the right one, and assume knowledge of p_{gL}, ρ_{gL}, u_{gL}, ϕ_{gL}, p_{sL} and u_{sL}. We also assume knowledge of ϕ_{gR}. By rearranging the Riemann invariants (7), we arrive at the following equation for the gaseous density on the right side of the solid contact line [13]:

$$F(\rho_{gR}) \equiv \frac{1}{2}\left(\frac{\mathscr{M}}{\phi_{gR}\rho_{gR}}\right)^2 + \frac{\gamma_g \eta_{gL} \rho_{gR}^{\gamma_g - 1}}{\gamma_g - 1} - \mathscr{E} = 0, \tag{8}$$

where

$$\mathscr{M} = \phi_{gL}\rho_{gL}(u_{gL} - u_{sL}), \tag{9}$$

$$\mathscr{E} = \frac{(u_{gL} - u_{sL})^2}{2} + \frac{\gamma_g}{\gamma_g - 1}\frac{p_{gL}}{\rho_{gL}}. \tag{10}$$

(Note that the knowledge of the left solid density is not required.)

The function F is not strictly monotone. It has a minimum at $\rho^* = \left(\frac{M^2}{\phi_{gR}^2 \gamma_g \eta_{gR}}\right)^{\frac{1}{\gamma_g + 1}}$. So if $F(\rho^*) > 0$ there is no solution to Eq. (8), if $F(\rho^*) = 0$ there is one solution, and if $F(\rho^*) < 0$ there are two solutions. In the latter case, it can be shown that the smaller of the two solutions implies that $(u_{gR} - u_{sR})^2 - c_{sR}^2 > 0$, whereas the larger one implies that $(u_{gR} - u_{sR})^2 - c_{sR}^2 < 0$. Andrianov and Warnecke [13] gave a criterion to select the admissible solution based on a continuity argument. This criterion requires that the signs of the term $(u_g - u_s)^2 - c_s^2$ have to be the same on both sides of the solid contact discontinuity. This condition will further be referred as the "*Andrianov and Warnecke criterion*".

We further proceed to present the jump (Rankine–Hugoniot) relations across shock waves. These relations can be obtained by noting that the balance equations for the mixture are in conservation form [14]. Also, by combining (1a) and (1g) we can obtain a hyperbolic conservation law for the solid density. In summary, we have,

$$\frac{\partial}{\partial t}\left(\sum_{k=g,s}\phi_k\rho_k\right) + \frac{\partial}{\partial x}\left(\sum_{k=g,s}\phi_k\rho_k u_k\right) = 0, \tag{11a}$$

$$\frac{\partial}{\partial t}\left(\sum_{k=g,s}\phi_k\rho_k u_k\right) + \frac{\partial}{\partial x}\left(\sum_{k=g,s}\phi_k\rho_k u_k^2 + \phi_k p_k\right) = 0, \tag{11b}$$

$$\frac{\partial}{\partial t}\left(\sum_{k=g,s}\phi_k\rho_k E_k\right) + \frac{\partial}{\partial x}\left(\sum_{k=g,s}\phi_k u_k(\rho_k E_k + p_k)\right) = 0, \tag{11c}$$

$$\frac{\partial \rho_s}{\partial t} + \frac{\partial}{\partial x}(\rho_s u_s) = 0, \tag{11d}$$

$$\frac{\partial}{\partial t}\left(\sum_{k=g,s}\phi_k\rho_k\eta_k\right) + \frac{\partial}{\partial x}\left(\sum_{k=g,s}\phi_k\rho_k u_k\eta_k\right) \geqslant 0. \tag{11e}$$

These equations, supplemented by the continuity equations for each phase (1a), (1d) can yield the desired Rankine–Hugoniot relations:

$$[\phi_g \rho_g U_g] = 0, \tag{12a}$$

$$[\phi_s \rho_s U_s] = 0, \tag{12b}$$

$$\left[\phi_s\left(\rho_s U_s^2 + p_s\right)\right] + \left[\phi_g\left(\rho_g U_g^2 + p_g\right)\right] = 0, \tag{12c}$$

$$\left[\phi_s \rho_s U_s\left(h_s + \frac{U_s^2}{2}\right)\right] + \left[\phi_g \rho_g U_g\left(h_g + \frac{U_g^2}{2}\right)\right] = 0, \tag{12d}$$

$$[\rho_s U_s] = 0, \tag{12e}$$

$$\sum_{k=g,s} [\phi_k \rho_k \eta_k U_k] \geqslant 0, \tag{12f}$$

where $[\cdot]$ denotes the jump of a quantity across the shock. Also, in the above expression, $U_s = u_s - u_D$ and $U_g = u_g - u_D$, with u_D being the shock speed.

If $U_s \neq 0$, that is if the discontinuity does not travel at the local solid phase speed u_s (12b) and (12e) yield: $[\phi_s] = 0$. In this case the non-conservative products are zero on both sides of the shock and, therefore, the balance laws of the two phases decouple from one another. Moreover, in the absence of non-conservative products, these balance laws constitute a system of hyperbolic conservation laws. The jump relations for this system are the following:

$$[\phi_g \rho_g U_g] = 0, \tag{13a}$$

$$\left[\phi_g\left(\rho_g U_g^2 + p_g\right)\right] = 0, \tag{13b}$$

$$\left[\phi_g \rho_g U_g\left(h_g + \frac{U_g^2}{2}\right)\right] = 0, \tag{13c}$$

$$[\phi_s \rho_s U_s] = 0, \tag{13d}$$

$$\left[\phi_s\left(\rho_s U_s^2 + p_s\right)\right] = 0, \tag{13e}$$

$$\left[\phi_s \rho_s U_s\left(h_s + \frac{U_s^2}{2}\right)\right] = 0, \tag{13f}$$

$$[\phi_s] = 0, \tag{13g}$$

$$\sum_{k=g,s} [\phi_k \rho_k \eta_k U_k] \geqslant 0. \tag{13h}$$

These relations are the classical Rankine–Hugoniot relations of gas dynamics written for each phase. In particular, the jump in one phase is totally independent of the flow variables of the other phase. So generally, across a shock, the state of one phase will be discontinuous while the state of the other phase will remain constant. Obviously, one can expect particular cases where a solid shock and a gaseous shock coincide.

On the other hand, when $U_s = 0$, that is if the discontinuity moves at the local solid particle speed, the system reduces to

$$[u_s] = 0, \tag{14a}$$

$$[\phi_g \rho_g (u_g - u_s)] = 0, \tag{14b}$$

$$[\phi_s p_s + \phi_g p_g + \phi_g \rho_g (u_g - u_s)^2] = 0, \tag{14c}$$

$$\left[\phi_g \rho_g (u_g - u_s)\left(h_g + \frac{(u_g - u_s)^2}{2}\right)\right] = 0. \tag{14d}$$

This system of equations is similar to the system (7) for the invariants across the solid contact discontinuity, except for the fact that (14) has one degree of freedom more than (7) has. This is so because the gaseous entropy is not conserved across the shock, whereas it is conserved across a solid contact discontinuity.

3. Wave configurations

The solution to the Riemann problem consists of different uniform intermediate states between the initial left and right states, covering the entire $t \geqslant 0$ semi-plane. These states are separated by centered waves that can be either shocks or contact discontinuities or rarefactions of the solid or gaseous phases. For a system of N equations there are in general N waves. In this case, however, $\lambda_s^0 = u_s$ is a double eigenvalue and, therefore, there can be at most six waves and five intermediate states. For the numerical solution of the Riemann problem it is important to determine the configuration of the waves, *i.e.* their relative ordering. The analysis and grouping of the possible configurations is investigated in this section.

Let C_g^0 and C_s^0 denote the gaseous and solid contact discontinuity, respectively. Since $\lambda_g^0 > \lambda_g^-$ and $\lambda_g^0 < \lambda_g^+$, the gaseous contact C_g^0 will always lie between the other two waves associated with the gaseous phase. Let C_g^- and C_g^+ denote the gaseous waves on the left and right of the gaseous contact, respectively. They can be either shocks or rarefactions. Similarly, the solid contact will lie between the other two waves of the solid phase C_s^-, C_s^+, which can also be either shocks or rarefactions.

It is obvious that the number of possible wave configurations can be very large. This is probably the main difficulty in the development of an efficient Riemann solver for the system of Eq. (1). Nevertheless, the characteristic analysis of our system shows that, across the various waves, the flow variables of one phase evolve independently of the variables of the other phase, except in the case of the solid contact discontinuity. In particular, the solid volume fraction ϕ_s remains constant across the solid and gaseous rarefactions and across the gaseous contact. It also remains constant across a gaseous shock that does not propagate at the solid velocity, *i.e.* when $U_s \neq 0$. Later in this section we show that $U_s = 0$ is possible only when the gaseous shock coincides with the solid contact discontinuity, which is a very special case.

From the above, it becomes clear that there is a simple way to classify the possible wave configurations based on the relative position of the solid contact discontinuity, C_s^0. And since C_s^0 lies always between C_s^- and C_s^+, one has only to take account of the relative position of C_s^0 with respect to the waves of the gaseous phase.

At this stage we will make the distinction between configurations for which the solid contact does not coincide with a gaseous wave, and configurations for which it does. The former ones will be referred to as *principal configurations* because these are the configurations that are encountered most of the time. The later ones will be referred to as *special configurations*, since they arise only in special circumstances, for example, when two eigenvalues coalesce.

3.1. Principal configurations

Let s_L, g_L denote the gaseous and solid states on the left of the initial discontinuity (*i.e.* along $x < 0$, $t = 0$) and s_R, g_R denote the states on its right, (*i.e.* along $x > 0$, $t = 0$). The intermediate states from left to right are denoted by s_1, g_1, s_2, g_2, *etc*.

There are four different principal configurations, namely Configurations 1, 2, 1′ and 2′. They are represented schematically in Fig. 1. In Configuration 1, C_s^0 lies on the left of C_g^-. In Configuration 2, C_s^0 lies between C_g^- and C_g^+. Finally, Configurations 1′ and 2′ are symmetric to Configurations 1 and 2, respectively.

For each principal configuration, we can establish certain relations between the intermediate states on the basis of the particular wave ordering. These relations will then be used in the proposed Riemann solver. For the sake of brevity, we present the relations that hold for Configurations 1 and 2 only. The relations for Configurations 1′ and 2′ are determined easily by using their symmetry to Configurations 1 and 2.

3.1.1. Configuration 1

First suppose that the C_g^- wave is a rarefaction. By definition the solid contact discontinuity C_s^0 is on the left of C_g^-. At the head of this rarefaction the "$-$" gaseous characteristic equals to $u_{g1} - c_{g1}$ and at the tail it equals to $u_{g2} - c_{g2}$; see Fig. 1 for notations. Hence Configuration 1 is admissible only if $u_{g1} - c_{g1}$ is larger than the speed of the solid contact discontinuity $u_{s1} = u_{s2}$:

$$u_{g1} - c_{g1} > u_{s1}. \tag{15}$$

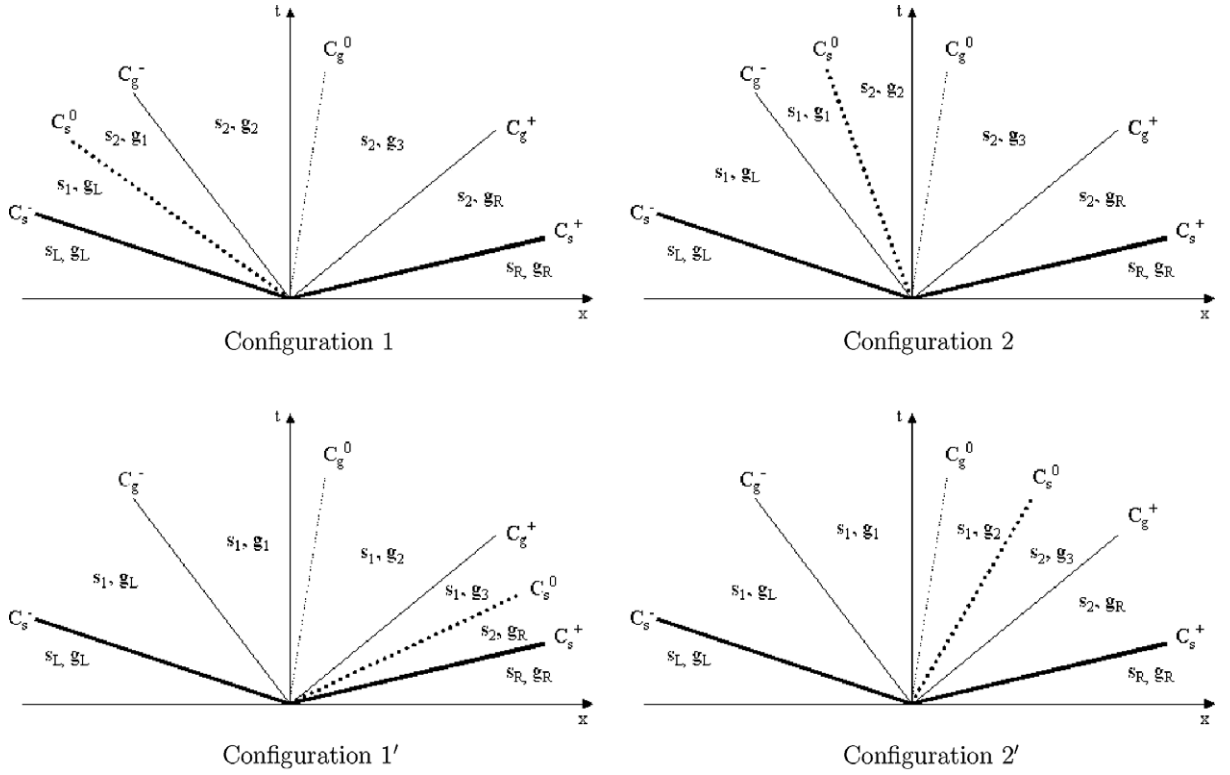

Fig. 1. Principal wave configurations. Bold lines indicate shocks or rarefactions of the solid phase. Bold dotted lines indicate contact discontinuities of the solid phase. Thin lines indicate shocks or rarefactions of the gaseous phase. Thin dotted lines indicate contact discontinuities of the gaseous phase.

Thus: $u_{g1} > u_{s1} + c_{g1} > u_{s1}$, and therefore

$$u_{g1} > u_{s1} \Longleftrightarrow u_{gL} > u_{s1}, \tag{16}$$

by virtue of the invariant ψ^0_{s3}, Eq. (7c); see relative discussion in Section 2. This means that the gaseous phase travels across the solid contact discontinuity from left to right.

Next suppose that the C_g^- wave is a shock. According to the Lax admissibility criterion, Lax [19], a shock is admissible if the characteristics on both sides of the shock impinge on it. Thus,

$$u_{g1} - c_{g1} > u_D > u_{s1}, \tag{17}$$

with u_D being the shock speed.

In conclusion, the following condition should always hold for Configuration 1,

$$u_{g1} - c_{g1} > u_{s1}. \tag{18}$$

By combining this equation with the Andrianov and Warnecke criterion, Section 2, we easily deduce that the admissible root of (8) in Configuration 1 is the smallest one.

3.1.2. Configuration 2

A similar analysis as above can be performed for this configuration also. The result is that for this configuration to be admissible, the following conditions should hold for C_g^- being either a rarefaction or a shock:

$$u_{g1} - c_{g1} < u_{s1}. \tag{19}$$

In other words, across the solid contact discontinuity, the speed of the gaseous phase relative to the solid phase is subsonic. Further, by combining this equation with the Andrianov and Warnecke criterion, we easily deduce that the admissible root of (8) in Configuration 2 is the largest one.

On the other hand, by definition of Configuration 2, the speed of the solid contact discontinuity is on the left of the gaseous one. Hence,

$$u_{s1} < u_{g2}. \tag{20}$$

This condition implies that, by virtue of the invariant ψ^0_{s3}, *cf.* Eq. (7c), the following is true,

$$u_{s1} < u_{g2}. \tag{21}$$

In other words, the gaseous phase crosses the solid contact discontinuity from left to right.

We conclude this subsection by noting that for Configurations 1′ and 2′ the inequalities (18), (19) and (21), respectively, are reversed.

3.2. Special configurations

3.2.1. Coalescence of solid and gaseous contact discontinuities

When the two contact lines coalesce, then the two phasial velocities are equal, $u_s = u_g$, and λ^0_s becomes a triple eigenvalue, $\lambda^0_s = \lambda^0_g (= u_g)$. However, the associated eigenvectors still provide a basis for $\mathscr{R}^7$. The coalescence of the eigenvalues also implies loss of an intermediate state in the Riemann problem (the state that lies between the two contacts in Configuration 2 or 2′).

With a straightforward calculation we find that the Riemann invariants across this "double" contact line are

$$\psi^0_{s,g1} = u_s, \tag{23a}$$

$$\psi^0_{s,g2} = u_g, \tag{23b}$$

$$\psi^0_{s,g3} = p_g, \tag{23c}$$

$$\psi^0_{s,g4} = \phi_s p_s + \phi_g p_g. \tag{23d}$$

Due to the coalescence of the eigenvalues, relations (23a) and (23b) become identical. The above three Riemann invariants, supplemented by the relation $u_g = u_s$, suffice to determine the intermediate states in a Riemann problem whenever the two contact lines coincide.

This particular configuration can only occur under very specific initial conditions. Further, numerically, such a case is quite unlikely to be encountered because of the finite precision of the calculations in iterative procedures and because of round-off errors. Nevertheless, this special configuration has been included in the proposed Riemann solver for the sake of completion.

3.2.2. Gaseous shock travelling at the solid phase velocity

This is the case when $U_s = u_s - u_D = 0$ and the solid volume fraction may jump across the shock. (Recall that if $U_s \neq 0$, ϕ_s then remains constant across the shock and the non-conservative products become classical functions thus allowing the derivation of the standard Rankine–Hugoniot relations as given in Section 2.) First, we show that a gaseous shock can travel at the solid phase velocity only when it coincides with a solid contact discontinuity. Suppose that the gaseous shock lies at the left of the C^-_s wave. The state on the left of C^-_s is denoted by "L". The shock then propagates with a speed $u_D = u_{sL}$. If the C^-_s wave is a rarefaction, the "–" characteristic at its head equals to $u_{sL} - c_{sL}$ and it has to be larger than the gaseous shock speed. Thus: $u_{sL} - c_{sL} > u_{sL}$. This is of course impossible because it implies a negative speed of sound. If the C^-_s wave is a shock, we arrive at the same inequality by applying directly the Lax admissibility criterion. In conclusion, a gaseous shock travelling at the local solid phase velocity cannot lie on the left of the C^-_s wave. A similar analysis leads us to the conclusion that such a shock cannot lie on the right of the C^+_s wave.

The only remaining possibility is for the shock to lie between the C^-_s and C^+_s waves. In this case the solid velocity between C^-_s and C^+_s becomes the speed of both the gaseous shock and the solid contact discontinuity. In summary, the case where $U_s = 0$ occurs only when the gaseous shock and the solid contact discontinuity coincide.

As mentioned above, when $U_s = 0$ the solid volume fraction may jump across the shock. Thus the non-conservative products are not classical functions anymore and standard jump conditions across the shock can not

be derived. Nevertheless, as mentioned in [14], Eq. (14) remain valid and define a three-dimensional manifold in $\mathscr{R}^7$. The invariants (7) across a solid contact are embedded in this manifold but they require that $[\eta_g = 0]$, hence solutions satisfying (7) can not be classified as gaseous shocks. This implies that the determination of the intermediate states in this particular configuration requires additional insight on the physical properties of this discontinuity and new theoretical results on hyperbolic non-conservative equations. Nevertheless, it is unlikely that this configuration occurs during numerical simulations because it requires that the shock speed and the solid contact speed must be equal down to machine precision, just as in the case of coinciding contact line discontinuities.

3.2.3. Solid contact discontinuity inside a gaseous rarefaction

In this case we have, $\lambda_s^0 = \lambda_s^{\pm}$, and the λ_s^0 becomes again a triple eigenvalue. Here, however, the eigenvectors of the system do not span the space $\mathscr{R}^7$ [14]. This is a case of parabolic degeneracy. Hyperbolic systems with parabolic degeneracies arise in elasticity theory, Keyfitz and Kranzer [20,21] oil reservoir simulation, Schaeffer and Shearer [22], Isaacson and Temple [23], *etc*. The equations can exhibit non-linear resonance at points with such degeneracies.

As regards the two-phase flow models of interest, in [13] it has shown that when $\lambda_s^0 = \lambda_s^{\pm}$, the volume fraction remains constant across the solid contact discontinuity, $[\phi_s] = 0$. (The gaseous pressure, density and entropy also remain constant across the solid contact.) This corresponds to a completely decoupled case. In other words, the Riemann problem is decoupled to two independent one-phase Riemann problems.

4. Description of the exact Riemann solver

In this section we present the structure and implementation of the proposed exact Riemann solver. First, we determine whether there is an initial discontinuity on the volume fraction ϕ_s. As mentioned above, if there is no such discontinuity then ϕ_s is constant on the entire $t \geqslant 0$ semi-plane and the two phases evolve independently. In this case, the Riemann problem decouples to two independent single-phase ones. Each of these two problems is solved with the Riemann solver of Collela and Glaz [24], which can treat a large class of convex equations of state. (The special configuration of a solid contact inside a gaseous rarefaction that was discussed in Section 3.2 is dealt precisely in this manner.)

If there is an initial discontinuity on ϕ_s, the proposed Riemann solver performs a sequential investigation of the principal wave configurations with the order $2 \to 2' \to 1 \to 1'$, until an admissible solution is calculated. In the following we describe the methodology of resolution for Configurations 1 and 2 only; Configurations $1'$ and $2'$ are solved in a completely analogous way.

4.1. Configuration 1

The objective is to determine the flow variables (pressure, density, velocity and volume fraction) for each phase in the intermediate states, given the initial left and right states s_L, s_R and g_L, g_R; see Fig. 1. The most difficult point is the calculation of the states of the two phases on one side of the solid contact discontinuity, provided that the states on the other side are known.

First we note that it is trivial to find the solid volume fraction in the intermediate states. As mentioned in Section 3, ϕ_s changes only across the solid contact discontinuity. Therefore, $\phi_{s1} = \phi_{sL}$ and $\phi_{s2} = \phi_{sR}$. (The gaseous volume fraction is calculated directly from the saturation condition, once ϕ_s is known). Further, in this configuration, the state of the gaseous phase on the left side of the solid contact discontinuity is already known, and equals to the initial left gaseous state g_L.

Now let us assume that the solid velocity u_{s1} is known. Then, the solid pressure p_{s1} and density ρ_{s1} can be determined by employing the relations that hold across the C_s^- wave. If this wave is a rarefaction, *i.e.* $u_{sL} < u_{s1}$, we employ thus Eq. (4) for ψ_s^-. If C_s^- is a shock, *i.e.* $u_{sL} > u_{s1}$, we employ the jump relations (13). This completes the calculation of the states on the left of the solid contact discontinuity.

We can then proceed to determine the states on its right by employing Eq. (7). In particular, according to (7a), the solid phase velocity is conserved, $u_{s2} = u_{s1}$, thus we can subsequently apply the relations that hold across the C_s^+ wave to determine p_{s2} and ρ_{s2}. To be more specific, we employ Eq. (4) for ψ_s^+ if $u_{s2} < u_{sR}$, and Eq. (13) if $u_{s2} > u_{sR}$. Hence the intermediate solid states s_1 and s_2 become known.

Thus, the solution up to this point can be parameterized with respect to u_{s1} (which was initially assumed as known). In other words, we can set up an iterative procedure based on u_{s1} to compute the solution up to this point. The criterion of convergence of this iteration is the solid pressure p_{s2} because there are two ways to compute this variable. The first way is via Eq. (7) once the states s_1 and g_1 are computed. (Note that state g_1 is calculated from Eq. (7) that hold across this contact. If two solutions exist for the system (7), the admissible one is the smallest one; see relative discussion in Section 3.) The second way is via the relations that hold across the C_s^+ wave (and the fact that $u_{s2} = u_{s1}$). This iteration terminates once the two different numerical predictions for p_{s2} become equal, or when we arrive at a non-admissible value for u_{s1} (see discussion below).

It remains to calculate the gaseous states g_2 and g_3 that lie on the right of the solid contact. In fact, from g_1 to g_R we have a classical single-phase Riemann problem, with g_1 playing the role of the "initial" left state. This problem is solved with the Riemann solver of Collela and Glaz [24], in which the relations that hold across the waves are parameterized with p_{g2}. In the iterative procedure that is set up with respect to p_{g2} the gaseous velocity u_{g3} can be determined in two different ways, and the iteration terminates once the two numerical predictions of u_{g3} become equal.

In conclusion, Configuration 1 can be resolved numerically with two independent iterations based on u_{s1} and p_{g2}, respectively. In the present implementation, the secant method is used for these iterations because it does not need an analytical expression for the derivatives of the functions involved. On the other hand, this method requires two initial estimates for each of the parameterizing variables u_{s1} and p_{g2}. Initial estimates for p_{g2} are determined according to the suggestions of Fryxell et al. [25].

The determination of initial estimates for u_{s1} is more delicate because not all values of u_{s1} are admissible. In particular, it is possible that, for certain values of u_{s1}, Eq. (8) does not admit a solution. As mentioned in Section 2, there will be no solution to (8) if $F(\rho^*) > 0$ with $\rho^* = \left(\frac{M^2}{\phi_{g1}^2 \gamma_g \eta_{g1}}\right)^{\frac{1}{\gamma_g+1}}$ for the case where the gaseous state is a perfect gas. By expanding $F(\rho^*)$ we obtain:

$$
\begin{aligned}
F_{\min} \equiv F(\rho^*) &= \frac{1}{2}\left(\frac{\mathscr{M}}{\phi_{g1}\rho^*}\right)^2 + \frac{\gamma_g}{\gamma_g - 1}\eta_{g1}\left(\frac{\mathscr{M}^2}{\phi_{g1}^2\gamma_g\eta_{g1}}\right)^{\frac{\gamma_g-1}{\gamma_g+1}} - \mathscr{E} \\
&= \mathscr{M}^{2\frac{\gamma_g-1}{\gamma_g+1}}\left(\frac{1}{2}\frac{(\phi_{g1}^2\gamma_g\eta_{g1})^{\frac{2}{\gamma_g+1}}}{\phi_{g1}^2} + \frac{\gamma_g}{\gamma_g-1}\frac{\eta_{g1}}{\left(\phi_{g1}^2\gamma_g\eta_{g1}\right)^{\frac{\gamma_g-1}{\gamma_g+1}}}\right) - \mathscr{E},
\end{aligned}
\tag{24}
$$

where

$$
\mathscr{M} = \phi_{gL}\rho_{gL}(u_{gL} - u_{s1}), \tag{25}
$$

$$
\mathscr{E} = \frac{(u_{gL} - u_{s1})^2}{2} + \frac{\gamma_g}{\gamma_g - 1}\frac{p_{gL}}{\rho_{gL}}. \tag{26}
$$

By defining a new constant

$$
K = (\phi_{gL}\rho_{gL})^{2\frac{\gamma_g-1}{\gamma_g+1}}\left(\frac{1}{2}\frac{\left(\phi_{g1}^2\gamma_g\eta_{g1}\right)^{\frac{2}{\gamma_g+1}}}{\phi_{g1}^2} + \frac{\gamma_g}{\gamma_g-1}\frac{\eta_{g1}}{\left(\phi_{g1}^2\gamma_g\eta_{g1}\right)^{\frac{\gamma_g-1}{\gamma_g+1}}}\right), \tag{27}
$$

Eq. (24) can be written as

$$
F_{\min} = K((u_{gL} - u_{s1})^2)^{\frac{\gamma_g-1}{\gamma_g+1}} - \frac{(u_{gL} - u_{s1})^2}{2} - \frac{\gamma_g}{\gamma_g - 1}\frac{p_{gL}}{\rho_{gL}}. \tag{28}
$$

This value has to be negative so that Eq. (8) admits a solution. In this expression all variables are known, except u_{s1}. In fact, $F_{\min}$ can be viewed as a function of the variable $\omega \equiv (u_{gL} - u_{s1})^2$. The properties of this function are:

$$
\begin{aligned}
&F_{\min}(0) = -\frac{\gamma_g}{\gamma_g - 1}\frac{p_{gL}}{\rho_{gL}},\\
&\lim_{\omega\to\infty} F_{\min}(\omega) = -\infty,\\
&\frac{dF_{\min}}{d\omega} = \frac{\gamma_g - 1}{\gamma_g + 1}K(\omega)^{\frac{-1}{\gamma_g+1}} - \frac{1}{2}.
\end{aligned}
\tag{29}
$$

The last relation implies that there is a maximum of $F_{\min}$, $F^*_{\min} \equiv F_{\min}(\omega^*)$, with

$$
\omega^* \equiv ((u_{gL} - u_{s1})^2)^* = \left(2\frac{\gamma_g - 1}{\gamma_g + 1}K\right)^{\frac{\gamma_g+1}{2}}. \tag{30}
$$

The admissible values for u_{s1} are those for which $F_{\min} \leqslant 0$. Thus,

- if $F^*_{\min} \leqslant 0$, then Eq. (8) admits a solution for any value of u_{s1}.
- if $F^*_{\min} > 0$, then Eq. (8) admits a solution for values of u_{s1} such that $\omega = (u_{gL} - u_{s1})^2$ does not lie between ω_0 and ω_1, with ω_0 and ω_1 being the zeros of $F_{\min}(\omega)$; see Fig. 2.

If $F^*_{\min} \leqslant 0$, we use the following initial estimates, $u^{(0)}_{s1} = u_{gL} - c_{gL}$ and $u^{(1)}_{s1} = u_{gL}$. If $F^*_{\min} > 0$, then we first seek initial estimates for u_{s1} in the range of $\omega \leqslant \omega_0$. The initial estimates of ω are $\omega^{(0)} = 0$ and $\omega^{(1)} = \omega_0$. Since in this configuration it is valid that $u_{s1} \leqslant u_{gL}$ (*cf.* (16)), the initial estimates for u_{s1} become $u^{(0)}_{s1} = u_{gL}$ and $u^{(1)}_{s1} = u_{gL} - \sqrt{\omega_0}$.

If the iteration does not converge for values of u_{s1} so that $\omega \leqslant \omega_0$, then we seek initial estimates for u_{s1} in the range of $\omega \geqslant \omega_1$. The initial estimates of ω are $\omega^{(0)} = \omega_1$ and $\omega^{(1)} = k\,\omega_1$, with $k > 1$. (The value $k = 1.3$ has worked well during our numerical experiments.) Thus, the initial estimates for u_{s1} become $u^{(0)}_{s1} = u_{gL} - \sqrt{\omega_1}$ and $u^{(1)}_{s1} = u_{gL} - k\sqrt{\omega_1}$.

If this iteration does not converge either, then Configuration 1 can not be a solution to the Riemann problem. Further, we note that not all values of u_{s1} are admissible. In particular u_{s1} must satisfy $u_{s1} < u_{gL} - c_{gL}$; see Section 3.1. If the iterative procedure for u_{s1} converges to a value that violates this condition, then again Configuration 1 can not be a solution to the Riemann problem.

4.2. Configuration 2

As in the previous configuration, the volume fractions change only across the solid contact discontinuity, so $\phi_{s1} = \phi_{sL}$, $\phi_{s2} = \phi_{sR}$ and ϕ_g is given by the saturation condition. The other flow variables in the intermediate states are calculated via two iterative procedures, an "exterior" one and an "interior" one.

The exterior iteration is based on p_{g1} and yields the values of ρ_{g1} and u_{g1} with the relations that hold across the C^-_g wave; see Fig. 1. These equations are (4) if C^-_g is a rarefaction, or Eq. (13) if C^-_g is a shock. The interior iteration is based on u_{s1} and yields the values of p_{s1} and ρ_{s1} using the equations of the C^-_s wave; (5) if it is a rarefaction or (13) if it is a shock. In this fashion the intermediate states on the left of the solid contact

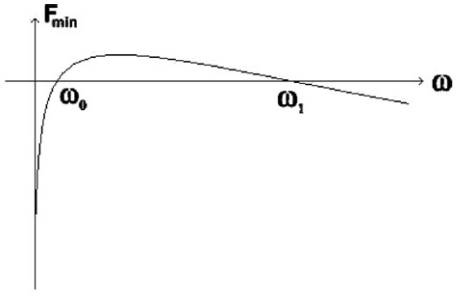

Fig. 2. Plot of $F_{\min}(\omega)$, $\omega = (u_{gL} - u_{s1})^2$.

discontinuity are computed. Next we calculate states s_2 and g_2 via the relations that hold across the C_s^0 and C_s^+. Further, state g_3 is calculated using the relations that hold across the C_g^+ wave and the fact that $p_{g3} = p_{g2}$.

The convergence criterion for the interior iteration is the solid pressure p_{s2} because there are two ways to compute this variable. The first way is via Eq. (7) once the states s_1 and g_1 are computed. The second way is via the relations that hold across the C_s^+ wave (and the fact that $u_{s2} = u_{s1}$).

The convergence criterion for the exterior iteration is the gaseous velocity u_{g3}, which can be calculated via the relations that hold across the C_g^+ wave, and via the relations that hold across the C_g^0 wave, Eq. (6a).

As in the previous configuration, certain admissibility conditions exist for u_{s1}. In fact, these conditions read the same as Eqs. (24)–(30), with g_L being replaced by g_1.

In conclusion, the iterative procedure works as follows :

- **Exterior iteration** :
- −Estimate p_{g1}. Next calculate ρ_{g1} and u_{g1}.
- −
  - **Interior iteration** :
  - −Estimate u_{s1}. Then calculate p_{s1} and ρ_{s1}.
  - −Calculate the variables on the right side of the solid contact discontinuity, $p_{g2}, \rho_{g2}, u_{g2}$ and u_{s2}.
  - −Calculate p_{s2} and ρ_{s2} from the relations for the C_s^+ wave.
  - −If the iteration has converged, then continue on the exterior iteration.
- −Calculate ρ_{g3} and u_{g3} from the relations for the C_g^+ wave.
- −If the iteration has converged, then a solution to the Riemann problem is found.

As regards the special configurations, we note that the case of solid contact discontinuity inside gaseous rarefaction is treated in the beginning of the solver when we examine if there is no discontinuity in ϕ_s. The case of coinciding contact discontinuities is examined explicitly if none of the four principal configurations have given a solution. Finally, the case of coinciding gaseous shock and solid contact is not treated as there is currently no solution available for this case; see discussion in Section 3.2.

We also note that the Riemann solver proposed herein does not include explicitly cases corresponding to vanishing phases. Numerical experiments have shown that these cases can be resolved in a satisfactory manner by assigning a very small value (*e.g.* 10^{-10}) as the lower limit to the volume fraction of the vanishing phase; see also Schwendeman et al. [18].

In order to examine the accuracy and robustness of the proposed algorithm we used the test cases employed by Andrianov and Warnecke [13] for their ''inverse Riemann solver''. (The inverse Riemann problem consists of finding the *initial* left and right states of the Riemann problem, given the intermediate states on the left and on the right of the solid contact discontinuity.) All five cases were accurately calculated by our Riemann solver.

5. Numerical methods for the integration of the non-conservative products

The presence of non-conservative products renders the numerical integration of the family of model (1) quite challenging. The reason is that, as mentioned in the introduction, non-conservative products do not represent flux terms and, therefore, must be integrated as source terms. But this can not be done in a straightforward manner because these products can only be defined in the sense of distributions on the cell interfaces.

By now, several approaches have been already proposed for the integration of the non-conservative products appearing in (1); namely Schwendeman et al. [18], Andrianov and Warnecke [13] and Braconnier of the Université Bordeaux [26]. It seems, however, that none of the existing methods is robust enough. In particular, spurious oscillations can arise when the solid contact discontinuity approaches another wave or when the initial conditions imply significant jumps in ϕ; see [13].

In this section we describe the first and second-order versions of the method proposed in [18]. Henceforth it is referred to as ''Method 1''. It is based on exploiting information from the local Riemann solver that is solved

on the cell interfaces in finite-volume algorithms. In [18] the authors integrate the non-conservative products by assuming a smooth evolution of the variables inside a vanishingly thin solid contact discontinuity. Herein we present an alternative formulation which is based on the representation of the solid volume fraction as a Heavyside function. The final equations are the same as in [18]. Later in this article, the accuracy and robustness of the first-order version of this method will be compared to those of [13,26]. For this reason, we provide a brief description of these methods, too. Henceforth they are referred to as "Method 2" and "Method 3", respectively.

First-order methods are in general too diffusive to be considered as sufficiently accurate. It is therefore important to test the possibility of extending them to second-order accuracy. The implementation of Method 1 in second-order algorithms (such as, for example, the MUSCL-type schemes, van Leer [27]) can be done in a relatively easy manner; see also Schwendeman et al. [18]. Note that in [13] it has already been shown that Method 2 could easily be extended to second-order, see [13] for more information. The extension of Method 3 to second-order accuracy is relatively complex in, and for this reason it will not be considered herein.

5.1. Method 1

We first describe the **first-order** version of Method 1. To this end, let us consider the standard Godunov scheme for the numerical integration of the system (1). Thus, the flow variables are approximated by piecewise constant functions and a local Riemann problem is solved on the cell interfaces to advance the solution in time.

Since the flow variables are constant inside each cell, the integrals of the non-conservative products can be non-zero only because of (possible) jumps of ϕ_s across the solid contacts emanating from the cell interfaces (on which a local Riemann problem is solved). Further, in the solution of the Riemann problem, the solid volume fraction ϕ_s is a Heavyside function. In order to fix ideas, let U denote the speed of the solid contact discontinuity and consider the change of variables $x' = x - Ut$. The expression for the solid volume fraction reads

$$\phi_s(x') = \phi_{sL} H(-x') + \phi_{sR} H(x'), \tag{31}$$

where $H(x)$ denotes the Heavyside function, ϕ_{sL}, ϕ_{sR} are the left and right initial values of ϕ_s and $U = u_{s1} = u_{s2}$. (The notations are the same as in Section 4; see Fig. 1.)

Further, in a small region around the solid contact discontinuity, the momentum equation for the solid phase is:

$$-U \frac{d}{dx'}(\phi_s \rho_s u_s) + \frac{d}{dx'}\left(\phi_s \rho_s u_s^2 + \phi_s p_s\right) = p_g \frac{d\phi_s}{dx'}. \tag{32}$$

But in this region we also have that $u_s = u_{s1} = u_{s2} = U$ is constant, see Eq. (7a). Thus, the last equation yields

$$\frac{d}{dx'}(p_s \phi_s) = p_g \frac{d\phi_s}{dx'}. \tag{33}$$

Using this result and Eq. (31), the non-conservative products of the system (1) read, at the vicinity of the solid contact line,

$$u_s \frac{\partial \phi_s}{\partial x} = u_s \frac{d\phi_s}{dx'} = (\phi_{sR} - \phi_{sL}) U \delta(x'), \tag{34}$$

$$p_g \frac{\partial \phi_s}{\partial x} = p_g \frac{d\phi_s}{dx'} = \frac{d(p_s \phi_s)}{dx'} = (\phi_{sR} p_{s2} - \phi_{sL} p_{s1}) \delta(x'), \tag{35}$$

$$p_g u_s \frac{\partial \phi_s}{\partial x} = p_g u_s \frac{d\phi_s}{dx'} = u_s \frac{d(p_s \phi_s)}{dx'} = (\phi_{sR} p_{s2} - \phi_{sR} p_{s1}) U \delta(x'). \tag{36}$$

where $\delta(x')$ denotes the Dirac function. Let Δx denote the length of a computational cell. For a time Δt sufficiently small the quantity $\Delta x - U\Delta t$ is positive and, therefore, the integrals of the non-conservative products over $\left[x_{i-\frac{1}{2}}, x_{i+\frac{1}{2}}\right] \times [t^n, t^{n+1}]$ are non-zero.

By taking into account the contributions of the solid contact lines emanating from both cell interfaces, we arrive at the following expressions

$$\int_{t^n}^{t^{n+1}} \int_{x_{i-\frac{1}{2}}}^{x_{i+\frac{1}{2}}} u_{\mathrm{s}} \frac{\partial \phi_{\mathrm{s}}}{\partial x} \mathrm{d}x = \Delta t (S^1_{i-1/2} - S^1_{i+1/2}), \tag{37}$$

$$\int_{t^n}^{t^{n+1}} \int_{x_{i-\frac{1}{2}}}^{x_{i+\frac{1}{2}}} p_{\mathrm{g}} \frac{\partial \phi_{\mathrm{s}}}{\partial x} \mathrm{d}x = \Delta t (S^2_{i-1/2} - S^2_{i+1/2}), \tag{38}$$

$$\int_{t^n}^{t^{n+1}} \int_{x_{i-\frac{1}{2}}}^{x_{i+\frac{1}{2}}} p_{\mathrm{g}} u_{\mathrm{s}} \frac{\partial \phi_{\mathrm{s}}}{\partial x} \mathrm{d}x = \Delta t (S^3_{i-1/2} - S^3_{i+1/2}), \tag{39}$$

with

$$S^1_{i-1/2} = \begin{cases} (\phi_{\mathrm{sR}} p_{\mathrm{s2}} - \phi_{\mathrm{s1}} p_{\mathrm{sL}})_{i-1/2}, & \text{if } U_{i-1/2} > 0, \\ 0, & \text{if } U_{i-1/2} < 0, \end{cases} \tag{40}$$

$$S^2_{i-1/2} = \begin{cases} (U(\phi_{\mathrm{sR}} p_{\mathrm{s2}} - \phi_{\mathrm{sL}} p_{\mathrm{s1}}))_{i-1/2}, & \text{if } U_{i-1/2} > 0, \\ 0, & \text{if } U_{i-1/2} < 0, \end{cases} \tag{41}$$

$$S^3_{i-1/2} = \begin{cases} (U(\phi_{\mathrm{sR}} - \phi_{\mathrm{sL}}))_{i-1/2}, & \text{if } U_{i-1/2} > 0, \\ 0, & \text{if } U_{i-1/2} < 0, \end{cases} \tag{42}$$

and

$$S^1_{i+1/2} = \begin{cases} (\phi_{\mathrm{sR}} p_{\mathrm{s2}} - \phi_{\mathrm{s1}} p_{\mathrm{sL}})_{i+1/2}, & \text{if } U_{i+1/2} < 0, \\ 0, & \text{if } U_{i+1/2} > 0, \end{cases} \tag{43}$$

$$S^2_{i+1/2} = \begin{cases} (U(\phi_{\mathrm{sR}} p_{\mathrm{s2}} - \phi_{\mathrm{sL}} p_{\mathrm{s1}}))_{i+1/2}, & \text{if } U_{i+1/2} < 0, \\ 0, & \text{if } U_{i+1/2} > 0, \end{cases} \tag{44}$$

$$S^3_{i+1/2} = \begin{cases} (U(\phi_{\mathrm{sR}} - \phi_{\mathrm{sL}}))_{i+1/2}, & \text{if } U_{i+1/2} < 0, \\ 0, & \text{if } U_{i+1/2} > 0. \end{cases} \tag{45}$$

All the quantities appearing in the above expressions are obtained as part of the solution of the local Riemann problem that is solved on each cell interface. These relations can be used directly in the first-order Godunov method, which reads

$$Q_i^{n+1} = Q_i^n - \frac{\Delta t}{\Delta x_i} \left(F^n_{i+\frac{1}{2}} - F^n_{i-\frac{1}{2}} \right) + \frac{\Delta t}{\Delta x_i} \left(\mathscr{S}^n_{i-\frac{1}{2}} - \mathscr{S}^n_{i+\frac{1}{2}} \right), \tag{46}$$

where

$$Q = \begin{bmatrix} \phi_{\mathrm{s}} \\ \phi_{\mathrm{s}}\rho_{\mathrm{s}} \\ \phi_{\mathrm{s}}\rho_{\mathrm{s}}u_{\mathrm{s}} \\ \phi_{\mathrm{s}}\rho_{\mathrm{s}}E_{\mathrm{s}} \\ \phi_{\mathrm{g}}\rho_{\mathrm{g}} \\ \phi_{\mathrm{g}}\rho_{\mathrm{g}}u_{\mathrm{g}} \\ \phi_{\mathrm{g}}\rho_{\mathrm{g}}E_{\mathrm{g}} \end{bmatrix}, \quad F = \begin{bmatrix} 0 \\ \phi_{\mathrm{s}}\rho_{\mathrm{s}}u_{\mathrm{s}} \\ \phi_{\mathrm{s}}(\rho_{\mathrm{s}}u_{\mathrm{s}}^2 + p_{\mathrm{s}}) \\ \phi_{\mathrm{s}}u_{\mathrm{s}}(\rho_{\mathrm{s}}E_{\mathrm{s}} + p_{\mathrm{s}}) \\ \phi_{\mathrm{g}}\rho_{\mathrm{g}}u_{\mathrm{g}} \\ \phi_{\mathrm{g}}(\rho_{\mathrm{g}}u_{\mathrm{g}}^2 + p_{\mathrm{g}}) \\ \phi_{\mathrm{g}}u_{\mathrm{g}}(\rho_{\mathrm{g}}E_{\mathrm{g}} + p_{\mathrm{g}}) \end{bmatrix}, \quad \mathscr{S} = \begin{bmatrix} S^1 \\ 0 \\ S^2 \\ S^3 \\ 0 \\ -S^2 \\ -S^3 \end{bmatrix}. \tag{47}$$

The fluxes F in the above relation are calculated directly from the solution of the Riemann problem at each cell interface.

We proceed with the description of the **second-order** version of this method. In particular, we are seeking a second-order numerical approximation of the integrals of the non-conservative products inside each computational cell at $t^{n+1/2}$. These integrals can be considered as the sum of two parts. The first parts are due to the discontinuities of ϕ_{s} across the solid contact lines that lie inside the ith cell at $t^{n+1/2}$. These parts equal to $S^k_{i+1/2} - S^k_{i-1/2}$ whose expressions were given in (40)–(45).

The second parts are due to the variation of ϕ_{s} inside the cell. Let us denote these parts by $\widehat{S}^k, k = 1, 2, 3$. A straightforward manner to approximate them is the following. Assume, for example, that at $t^{n+1/2}$ both the

solid contact lines emanating from interfaces of the ith cell are inside this cell. These lines divide this cell into three subintervals; see Fig. 3. (If there is only one solid contact line in the cell, then it is divided into two subintervals, and so on.) Along the left and right subintervals, *i.e.* along the segments between the cell interfaces and their corresponding solid contact lines, ϕ_s remains constant. Therefore, the integrals of the non-conservative products along these subintervals are zero. The integrals along the middle subinterval are approximated by assuming linear variation of the flow variables between the state on the right of the left solid contact line and the state on left of the right one. These states are calculated by the Riemann solver. (If there is only one solid contact line on the cell, say the one from the left interface, we consider the state on the right of the solid contact line and the state on the interface, and so on.) In conclusion, we have

$$\widehat{S}^1 \simeq \frac{1}{2}(\hat{u}_{s,i+1/2} + \hat{u}_{s,i-1/2})(\hat{\phi}_{s,i+1/2} - \hat{\phi}_{s,i-1/2}), \tag{48}$$

$$\widehat{S}^2 \simeq \frac{1}{2}(\hat{p}_{g,i+1/2} + \hat{p}_{g,i-1/2})(\hat{\phi}_{s,i+1/2} - \hat{\phi}_{s,i-1/2}), \tag{49}$$

$$\widehat{S}^3 \simeq \frac{1}{2}(\hat{p}_{g,i+1/2}\hat{u}_{s,i+1/2} + \hat{p}_{g,i-1/2}\hat{u}_{s,i-1/2})(\hat{\phi}_{s,i+1/2} - \hat{\phi}_{s,i-1/2}). \tag{50}$$

In the above equations, and if $U_{i+1/2} \geqslant 0$, the variables $\hat{u}_{s,i-1/2}$, $\hat{\phi}_{s,i-1/2}$ and $\hat{p}_{g,i-1/2}$ are taken from the state on the right of the solid contact that emanates from the left interface. Otherwise, they are taken from the state on the left interface. Similarly, if $U_{i+1/2} \leqslant 0$, the variables $\hat{u}_{s,i+1/2}$, $\hat{\phi}_{s,i+1/2}$ and $\hat{p}_{g,i+1/2}$ are taken from the state on the left of the solid contact that emanates from the right interface. Thus overall, we have,

$$\int_{t^n}^{t^{n+1}} \int_{x_{i-\frac{1}{2}}}^{x_{i+\frac{1}{2}}} u_s \frac{\partial \phi_s}{\partial x} \mathrm{d}x \simeq \Delta t(S^1_{i-1/2} - S^1_{i+1/2} + \widehat{S}^1), \tag{51}$$

$$\int_{t^n}^{t^{n+1}} \int_{x_{i-\frac{1}{2}}}^{x_{i+\frac{1}{2}}} p_g \frac{\partial \phi_s}{\partial x} \mathrm{d}x \simeq \Delta t(S^2_{i-1/2} - S^2_{i+1/2} + \widehat{S}^2), \tag{52}$$

$$\int_{t^n}^{t^{n+1}} \int_{x_{i-\frac{1}{2}}}^{x_{i+\frac{1}{2}}} p_g u_s \frac{\partial \phi_s}{\partial x} \mathrm{d}x \simeq \Delta t(S^3_{i-1/2} - S^3_{i+1/2} + \widehat{S}^3). \tag{53}$$

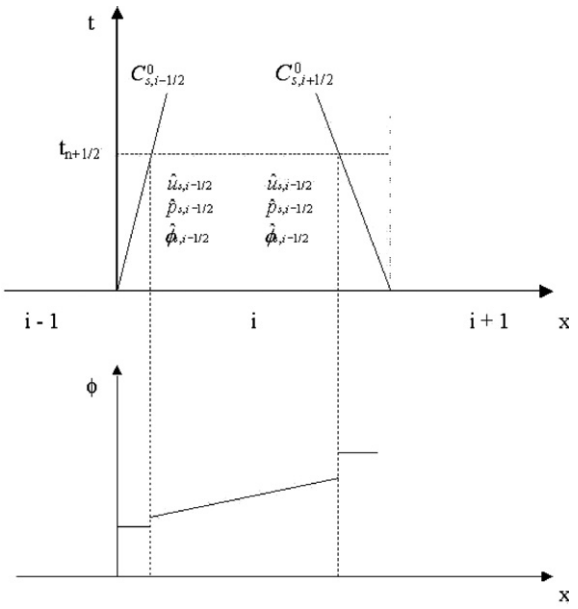

Fig. 3. Values of $\hat{u}_{s,i-1/2}$, $\hat{p}_{s,i-1/2}$, $\hat{\phi}_{s,i-1/2}$, $\hat{u}_{s,i+1/2}$, $\hat{p}_{s,i+1/2}$ and $\hat{\phi}_{s,i+1/2}$ for the second-order version of Method 1.

5.2. Method 2

This method is presented in [13] and is based on a criterion put forward by Abgrall [17]. According to this criterion, initially uniform pressure and velocity fields must remain uniform at all times. The integration of the non-conservative products are approximated as:

$$\int_{t^n}^{t^{n+1}} \int_{x_{i-\frac{1}{2}}}^{x_{i+\frac{1}{2}}} u_{\mathrm{s}} \frac{\partial \phi_{\mathrm{s}}}{\partial x} \mathrm{d}x \simeq u_{\mathrm{s},i}^{n} \left(\phi_{\mathrm{s},i+1/2}^{n+1/2} - \phi_{\mathrm{s},i-1/2}^{n+1/2} \right), \tag{54}$$

$$\int_{t^n}^{t^{n+1}} \int_{x_{i-\frac{1}{2}}}^{x_{i+\frac{1}{2}}} p_{\mathrm{g}} \frac{\partial \phi_{\mathrm{s}}}{\partial x} \mathrm{d}x \simeq \Delta t p_{\mathrm{g},i}^{n} \left(\phi_{\mathrm{s},i+1/2}^{n+1/2} - \phi_{\mathrm{s},i-1/2}^{n+1/2} \right), \tag{55}$$

$$\int_{t^n}^{t^{n+1}} \int_{x_{i-\frac{1}{2}}}^{x_{i+\frac{1}{2}}} p_{\mathrm{g}} u_{\mathrm{s}} \frac{\partial \phi_{\mathrm{s}}}{\partial x} \mathrm{d}x \simeq \Delta t p_{\mathrm{g},i}^{n} u_{\mathrm{s},i}^{n} \left(\phi_{\mathrm{s},i+1/2}^{n+1/2} - \phi_{\mathrm{s},i-1/2}^{n+1/2} \right). \tag{56}$$

The quantities $u_{\mathrm{s},i}^{n}$ and $p_{\mathrm{g},i}^{n}$ are the solid velocity and the gaseous pressure,respectively, in cell i at time $t = n\,\Delta t$. The quantities $\phi_{\mathrm{s},i+1/2}^{n-1/2}$ and $\phi_{\mathrm{s},i+1/2}^{n+1/2}$ are the solid volume fraction at the left and right cell interfaces, respectively, calculated with a Riemann solver at time $t = (n + 1/2)\Delta t$. An extension to second-order accuracy for this method can be found in [13].

5.3. Method 3

This method is based on solving local Riemann problems on the cell interfaces at time $t = (n + 1)\Delta t$. In order to fix ideas, let q be a "conservative" variable, ϕ_α, ρ_α, $\rho_\alpha u_\alpha$, $\rho_\alpha E_\alpha$, $\alpha = \mathrm{g}, \mathrm{s}$. The profile $\tilde{q}(x, t_{n+1})$ of q inside each cell can be constructed by piecing together the Riemann solutions. The solution can then be advanced in time by calculating the cell average of $\tilde{q}(x, t_{n+1})$,

$$q_i^{n+1} \simeq \frac{1}{\Delta x} \int_{x_{i-\frac{1}{2}}}^{x_{i+\frac{1}{2}}} \tilde{q}(x, t_{n+1}) \mathrm{d}x. \tag{57}$$

The advantage of this method is that it does not require the calculation of fluxes on the cell interfaces. Therefore, a direct numerical integration of the non-conservative products is not needed. On the other hand, this method is cumbersome to implement. Further, its extension to second-order accuracy is quite complex.

6. Numerical results

In this section, we present numerical results for four different shock-tube problems and compare the accuracy of the three methods presented above. The proposed Riemann solver is employed in all simulations. The computational domain is of length $L = 1$ and is divided uniformly in 300 cells. The CFL number is fixed at $\mathrm{CFL} = 0.8$. Further, the initial discontinuity is always located at $x = 0.5$.

6.1. Test 1

In this test, both phases are perfect gases with $\gamma_{\mathrm{s}} = \gamma_{\mathrm{g}} = 1.4$. The initial conditions are the following:

Phase α	$\phi_{\alpha \mathrm{L}}$	$u_{\alpha \mathrm{L}}$	$\rho_{\alpha \mathrm{L}}$	$p_{\alpha \mathrm{L}}$	$\phi_{\alpha \mathrm{R}}$	$u_{\alpha \mathrm{R}}$	$\rho_{\alpha \mathrm{R}}$	$p_{\alpha \mathrm{R}}$
s	0.4	0	1	1	0.8	0	2	2
g	0.6	0	0.5	1	0.2	0	1.5	2

Fig. 4 contains plots of the numerical results at time $t = 0.1$ obtained with Method 1. It can be observed that they are in good agreement with the exact solution, corresponding to configuration 2′. All contact discontinuities, shocks and rarefactions of each phase are well-captured. The results obtained with Methods 2 and 3

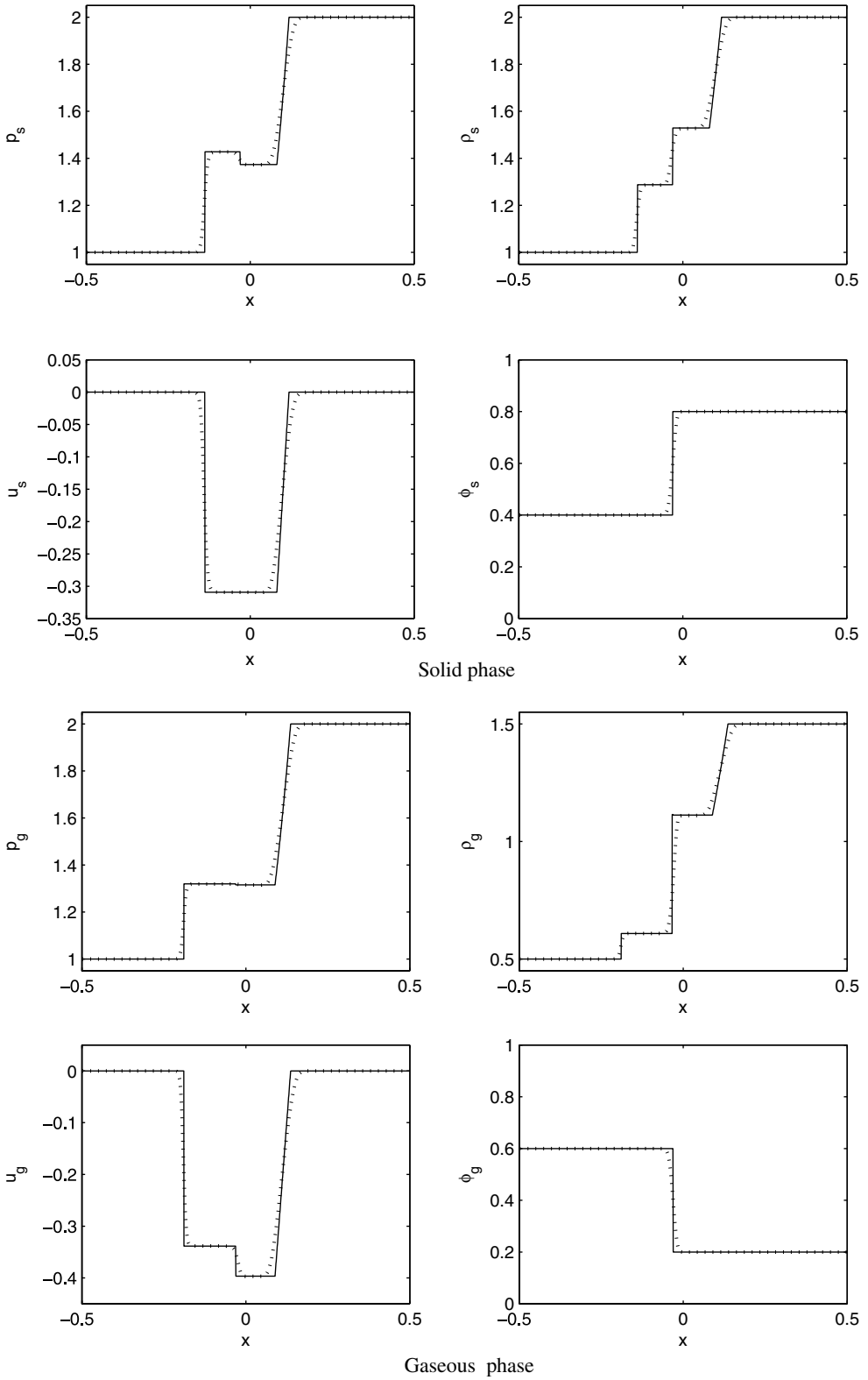

Fig. 4. Test 1. Exact solution (solid lines) and numerical first-order (dotted lines) solution obtained with Method 1 at $t = 0.1$.

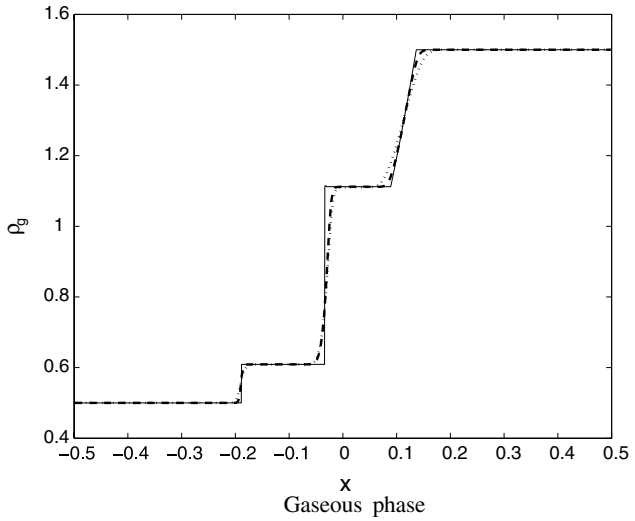

Fig. 5. Test 1. Exact solution (solid line) and numerical first-order (dotted line) and second-order (dashed line) solutions at $t = 0.1$.

are practically identical to those obtained with Method 1. For this reason, these results are not included in Fig. 4. This situation, *i.e.* all three first-order methods yielding identical results was observed in a large variety of initial conditions.

On the other hand, the second-order version of Method 1 provides, as expected, an improvement to the fidelity of the simulations. This can be clearly seen in Fig. 5 that contains plots of the gas density for the test case in hand.

6.2. Test 2

In this test case, the gaseous phase is a perfect gas with $\gamma_g = 1.4$, whereas the solid phase is a stiffened gas. Thus the equation of state of the solid phase reads,

$$e_s = \frac{p_s + \gamma_s \pi}{\rho_s(\gamma_s - 1)}, \tag{58}$$

where $\gamma_s = 3$ and $\pi = 100$.

The initial conditions are the following :

Phase α	$\phi_{\alpha L}$	$u_{\alpha L}$	$\rho_{\alpha L}$	$p_{\alpha L}$	$\phi_{\alpha R}$	$u_{\alpha R}$	$\rho_{\alpha R}$	$p_{\alpha R}$
s	0.4	0	800	500	0.3	0	1000	600
g	0.6	0	1.5	2	0.7	0	1	1

The exact solution at $t = 0.1$ and the results obtained with the second-order version of Method 1 are plotted in Fig. 6. In this figure it can be observed that the numerical solution is in good agreement with the exact one. Further, the smearing of discontinuities due to numerical diffusion is sufficiently small.

6.3. Test 3

In the third test, both phases are perfect gases with $\gamma_s = \gamma_g = 1.4$. The initial conditions are :

Phase α	$\phi_{\alpha L}$	$u_{\alpha L}$	$\rho_{\alpha L}$	$p_{\alpha L}$	$\phi_{\alpha R}$	$u_{\alpha R}$	$\rho_{\alpha R}$	$p_{\alpha R}$
s	0.8	0.3	2	5	0.3	0.3	2	12.8567
g	0.2	2	1	1	0.7	2.8011	0.1941	0.1

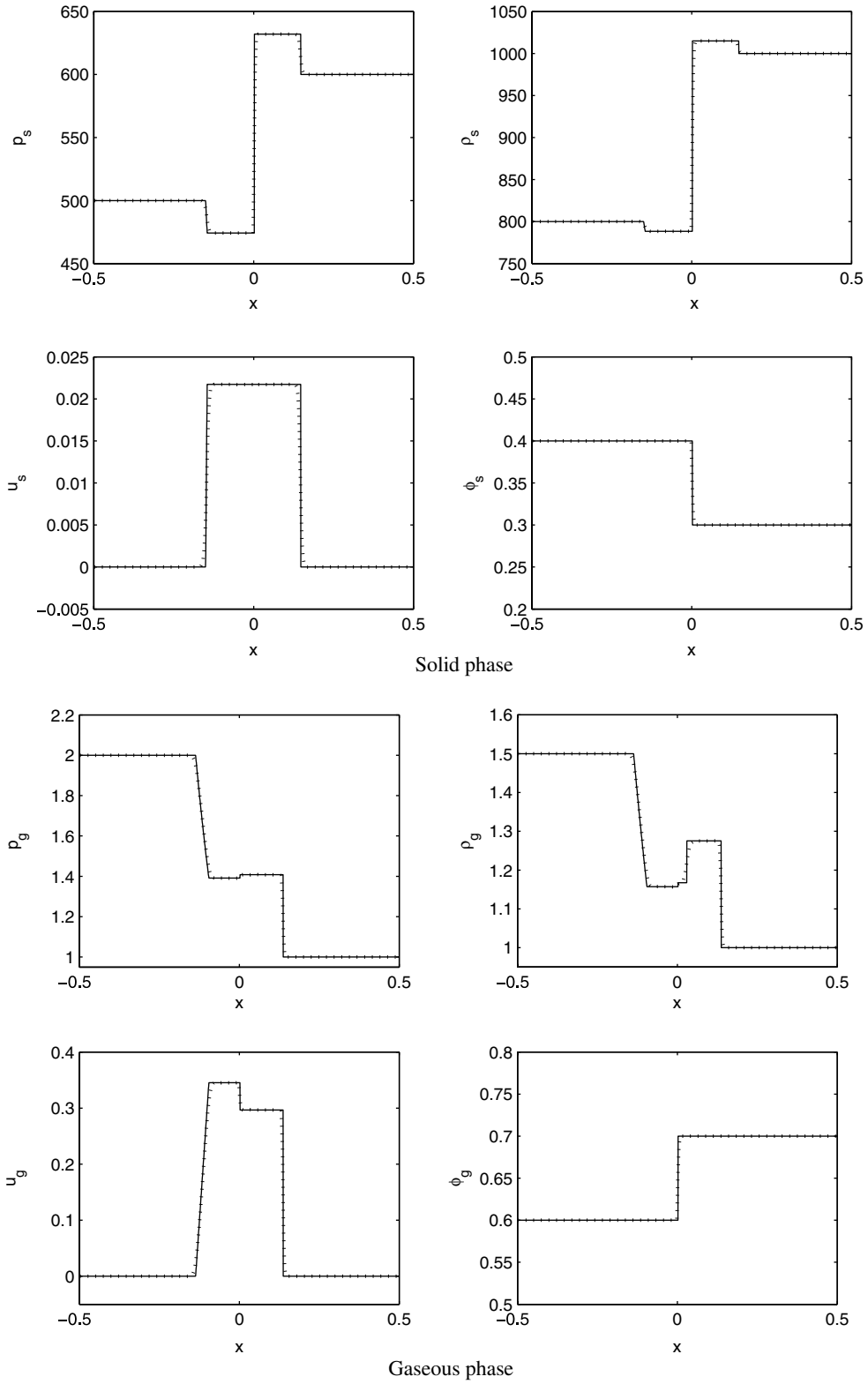

Fig. 6. Test 2. Exact solution (solid lines) and numerical solution (bold dotted lines) obtained with the second-order version of Method 1 at $t = 0.1$.

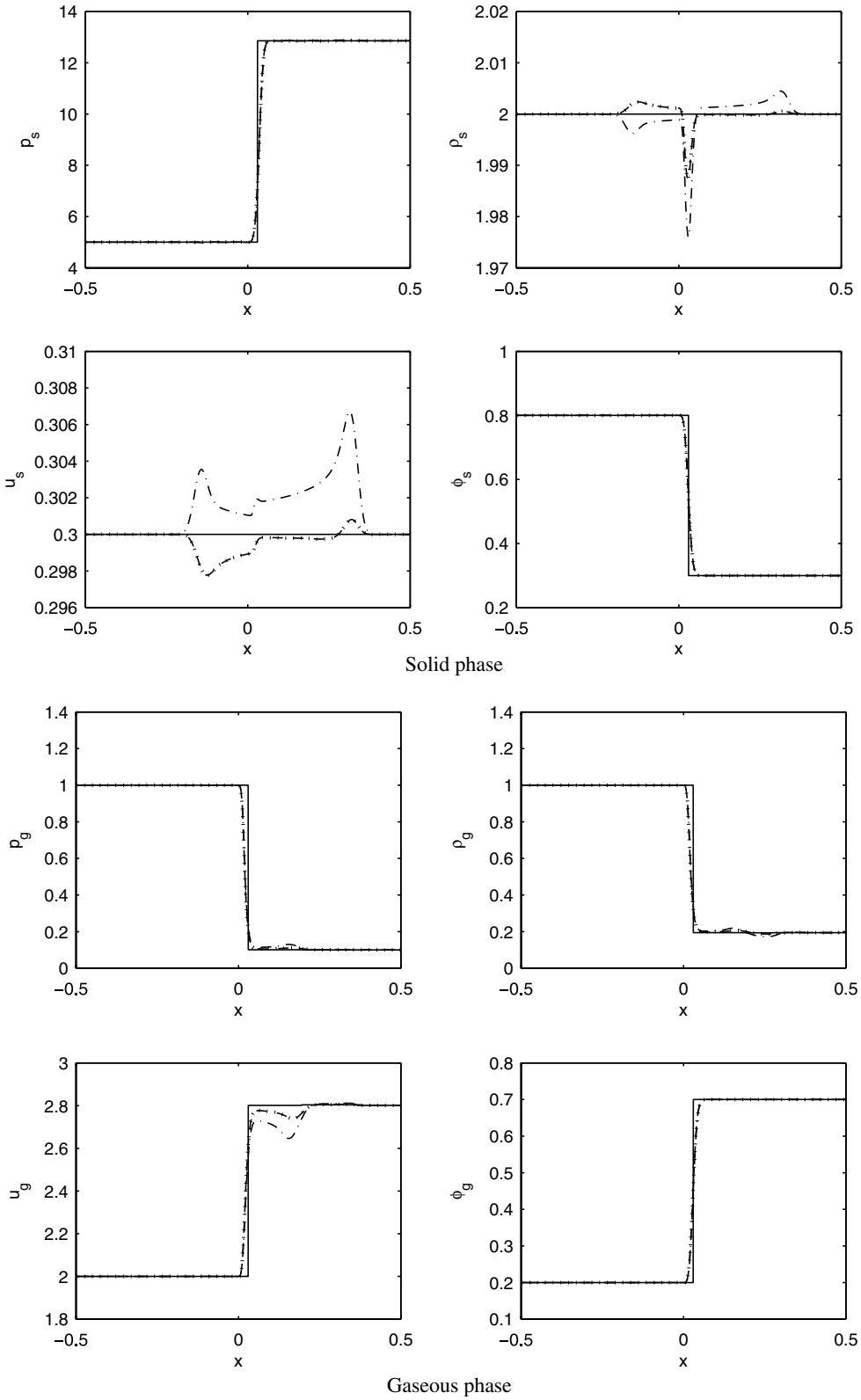

Fig. 7. Test 3. Exact solution (solid lines) and numerical solutions for Method 1 (bold dotted lines), Method 2 (thin dash-dotted lines) and Method 3 (thin dashed lines) at $t = 0.1$.

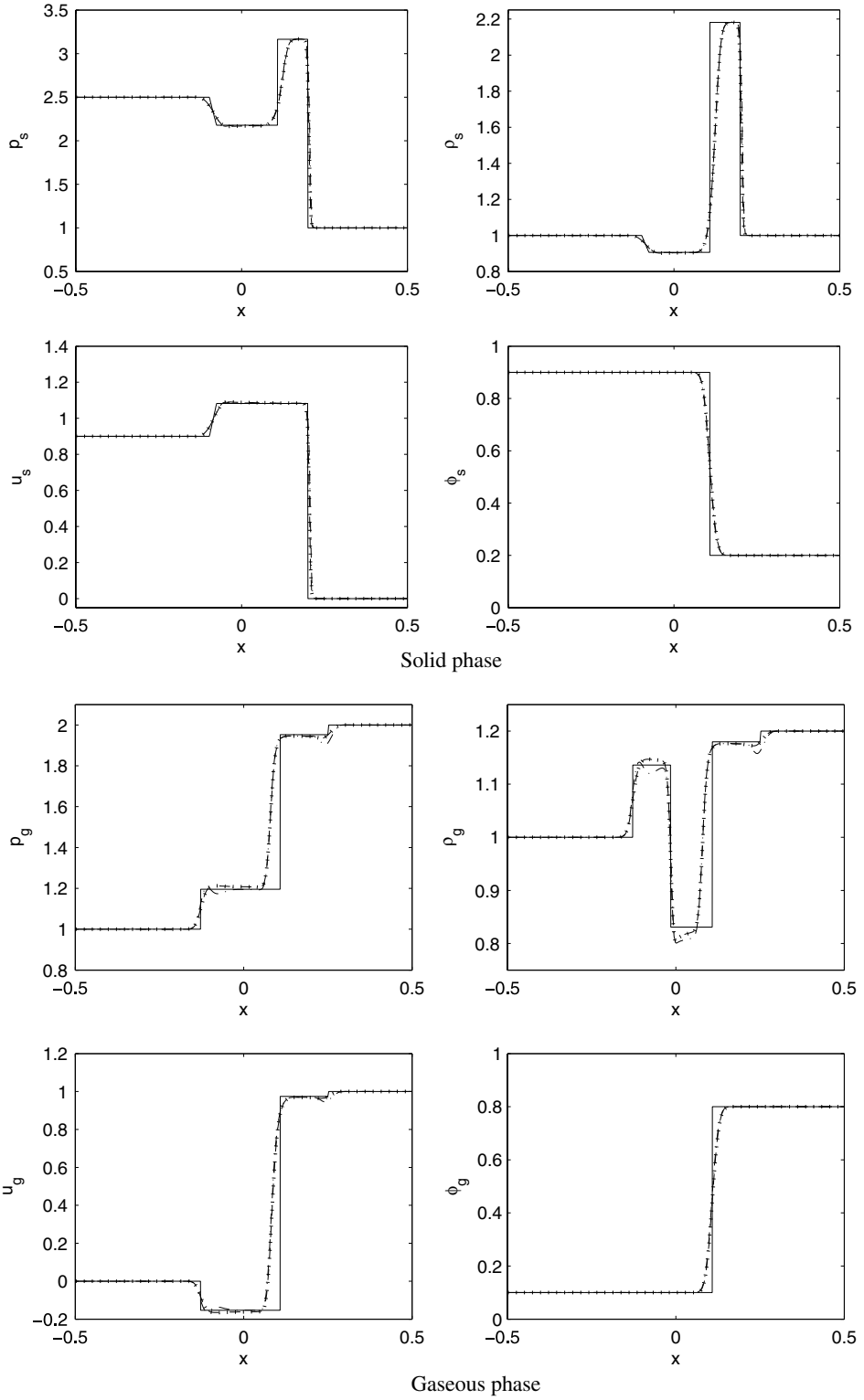

Fig. 8. Test 4. Exact solution (solid lines) and numerical solutions for Method 1 (bold dotted lines), Method 2 (thin dash-dotted lines) and Method 3 (thin dashed lines) at $t = 0.1$.

These conditions correspond to those of Test 1 in [13], and should produce a simple solid contact discontinuity, *i.e.* all other waves should vanish. This is a particularly challenging problem to simulate numerically; in [13] the authors employed Method 2 with an approximate Riemann solver and observed spurious oscillations in the numerical solution.

The numerical solutions are plotted in Fig. 7. It can be observed that the first-order version of Methods 1 and 3 produce practically identical results, whereas the results with Method 2 are less accurate. However, none of these methods deemed capable of producing results with negligible numerical artifacts. In fact, although these artifacts are small in the solid phase variables, they are significant in the gaseous phase variables, especially in the gas velocity field. More importantly, the spurious oscillations did not disappear with grid refinement.

6.4. Test 4

In the last test, both phases are again perfect gases with $\gamma_s = \gamma_g = 1.4$. The initial conditions are the following:

Phase α	$\phi_{\alpha L}$	$u_{\alpha L}$	$\rho_{\alpha L}$	$p_{\alpha L}$	$\phi_{\alpha R}$	$u_{\alpha R}$	$\rho_{\alpha R}$	$p_{\alpha R}$
s	0.9	0.9	1	3	0.2	0	1	1
g	0.2	0	1	1	0.8	1	1.5	2

These initial conditions constitute a difficult test, because they imply a strong discontinuity in the volume fraction. Fig. 8 contains plots of the exact solution, corresponding to Configuration 2′, and the numerical results obtained with the different methods.

Again, all of them produce numerical errors. These errors can be observed in the vicinity of the solid contact discontinuity, which is widely smeared, but also near the gaseous contact discontinuity across which the jump in the gas density is poorly calculated. By refining the grid to 1000 cells, it was observed that the solid contact discontinuity becomes less smeared, but the gas density near the gaseous contact is again poorly calculated; see Fig. 9. It is also interesting to mention that Methods 1 and 3 produced smaller errors than Method 2.

The numerical results in Tests 3 and 4 provide a strong indication that none of the three methods tested herein is sufficiently robust to handle strong volume fraction jumps. Thus, further study is needed to derive

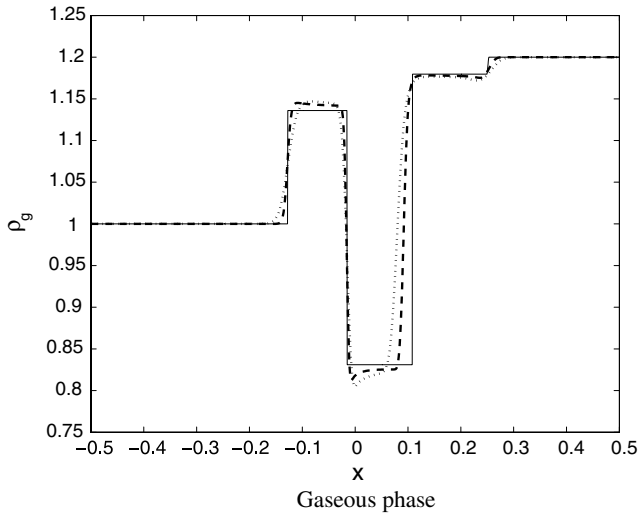

Fig. 9. Test 4. Exact solution (solid line) and numerical solutions for the gaseous density at $t = 0.1$ with $\Delta x = 1/300$ (dotted line) and $\Delta x = 1/1000$ (dashed line).

improved algorithms for integrating the non-conservative products that are sufficiently robust and do not produce spurious oscillations.

7. Discussion on the ill-posedness of the Riemann problem

As mentioned in Section 3, the solutions to the Riemann problem can be classified into four principal configurations; see Fig. 1. For each of these configurations there are certain admissibility criteria relative to the ordering of the waves, and to the Andrianov and Warnecke criterion, Eqs. (15)–(21). Once a configuration fulfills these criteria, then a solution to the Riemann problem exists from this configuration.

However, the admissibility criteria of each principal configuration are not mutually exclusive. Further, they do not cover the entire range of parameters involved. This simply means that there can be initial conditions for which the Riemann problem admits more than an unique entropy-satisfying solutions or for which it does not admit a solution at all. Thus, the Riemann problem can be ill-posed.

The numerical experiments of [13] confirmed that such initial conditions do exist. Cases of non-uniqueness or non-existence of solutions to the Riemann problem have also been predicted in our numerical simulations. As regards the non-uniqueness of solutions in particular, we observed that, under certain initial conditions, there was one solution from Configuration 1 and another one from Configuration 2, while for other initial conditions we would get one solution from $1'$ and another one from $2'$. Multiple solutions with other pairings of configurations were not predicted in our simulations.

To illustrate the issue of ill-posedness let us consider a shock tube problem with the following initial conditions, true

Phase α	$\phi_{\alpha L}$	$u_{\alpha L}$	$\rho_{\alpha L}$	$p_{\alpha L}$	$\phi_{\alpha R}$	$u_{\alpha R}$	$\rho_{\alpha R}$	$p_{\alpha R}$
s	0.5	u_{sL}	2.1917	3	0.9	−1.1421	0.6333	2.5011
g	0.5	−0.789	6.3311	1	0.1	−0.6741	0.4141	0.0291

We assume that both phases are ideal gases, with $\gamma_g = \gamma_s = 1.4$. All initial conditions are fixed, except the left solid phase velocity, u_{sL}. Numerical solutions to this problem are obtained for different values of u_{sL}. In Fig. 10 we represent schematically the principal configurations that converge to an admissible solution for the Riemann problem as the parameter u_{sL} varies.

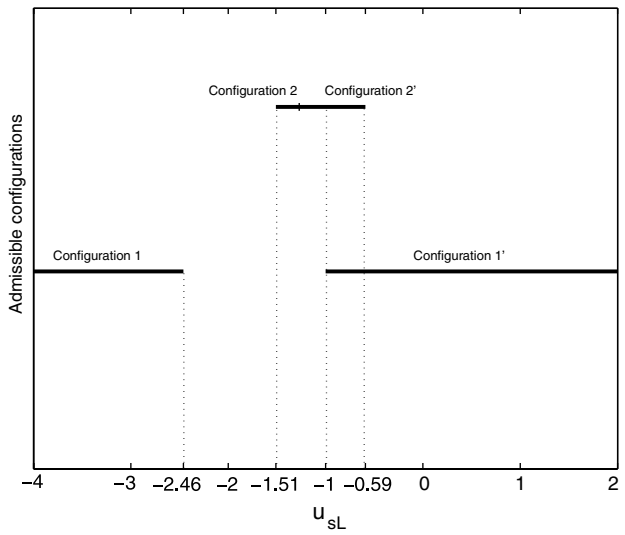

Fig. 10. Admissible configurations to the Riemann problem as a function of u_{sL}.

In this figure we can observe that when $-1.0 < u_{sL} < -0.59$, the solution is not unique. Instead, there are two solutions, from Configurations 1′ and 2′, respectively. Both solutions satisfy the entropy criterion. At this point it is interesting to mention that when $u_{sL} = -0.995$, the initial conditions correspond to those of Test 4 in [13], for which the authors observed differences between numerical results and exact solution. As a matter of fact, however, this is a case of existence of two solutions, and the numerical result in [13] simply corresponds to the second solution of the Riemann problem (see Fig. 11).

Non-uniqueness of solutions has also been encountered in the compressible, quasi-1D duct flow equations [13,28], in the shallow-water equations [29], and elsewhere. In sofar, various propositions have been put forward to select the physically relevant, "correct", solution when multiple solutions are present. In particular, the authors in [13] suggest that non-uniqueness of solutions in the quasi-1D duct flow model is due to the fact that this model can not describe multi-dimensional effects. Further, they compared solutions from the quasi-1D flow model with those obtained by multi-dimensional calculations and they concluded that the physically relevant solution corresponded to the maximal entropy increase. Thus, they proposed to employ the entropy-rate admissibility criterion of Dafermos [30]. According to this criterion, the correct solution is the one whose entropy increases at maximum rate.

This idea can be particularly relevant to two-phase flows because the duct-flow equations are really a special case of the two-phase flow models of interest. However, we note that the criterion of Dafermos [30] has been established for conservative systems. In particular, Dafermos has shown that in the case of such systems his criterion is completely equivalent to the viscosity criterion (according to which the correct solution should correspond to the viscous solution in the vanishing viscosity limit). Thus, for extending the Dafermos criterion in the two-phase flow models of interest, it would make sense to first apply the viscosity criterion, and then try to establish the equivalence between the two criteria. Such equivalence has not been demonstrated yet. Therefore, at the present time, there is not a firmly established criterion to select the physically more relevant solution.

Returning to the numerical example above, we observe that when $-2.46 < u_{sL} < -1.51$, there is no solution to the Riemann problem; see Fig. 10. Further numerical experiments predicted that initial conditions for which there is no solution are not special cases but do arise often. As another example, consider a shock tube problem in which there is no jump in the volume fraction, so $\phi_L = \phi_R$. This means that both phases are decoupled, and we can consider initial conditions such that the solid contact discontinuity lies inside a gaseous rarefaction. In this case there is an unique solution and it corresponds to the special configurations discussed in Section 3.2.

However, when perturbing slightly the volume fraction on one side, say $\phi_L = \phi_R + \varepsilon$ with ε an *arbitrarily* small value, then the Riemann problem does not admit a solution anymore. The non-existence of solutions for ε arbitrarily small indicates a pathological situation and, in our opinion, there are two possible explanations for it.

The first possible explanation is that the source terms of the two-phase flow models may influence the evolution of the initial condition immediately. Then, the solution of the non-homogeneous Riemann problem would not converge to the solution of the corresponding homogeneous one as time tends to zero. In other words, the slopes of the waves of the non-homogeneous problem at $t = 0$ do not coincide with the straight lines representing the centered waves of the homogeneous, self-similar problem. If this is the case, the design of numerical schemes for the two-phase models of interest should be based solely on the non-homogeneous Riemann problem.

The second possible explanation for the non-existence of solution is a fundamental breakdown of the validity of the two-phase models examined herein. In other words, it may be questionable whether such models are capable to describe physical phenomena in a sufficiently wide range of conditions. If this is the case, then one or more of the principal assumptions that were made in deriving these models are wrong. For example,

(i) The assumption that the volume fraction ϕ_s is enough to describe the micro-structure of the system might be incorrect. In fact, due to this assumption one finds that the solid phase does not support shear in equilibrium which is manifestly incorrect. Thus the viscosity of the solid phase, at least, should be taken into account even when compressibility effects are dominant. The two-phase model of Papalexandris [7] considers $\nabla\phi_s$ as an additional variable related to the microstructure of the mixture. The addition of this variable introduces non-Newtonian terms of the solid viscous-pressure tensor thus providing a

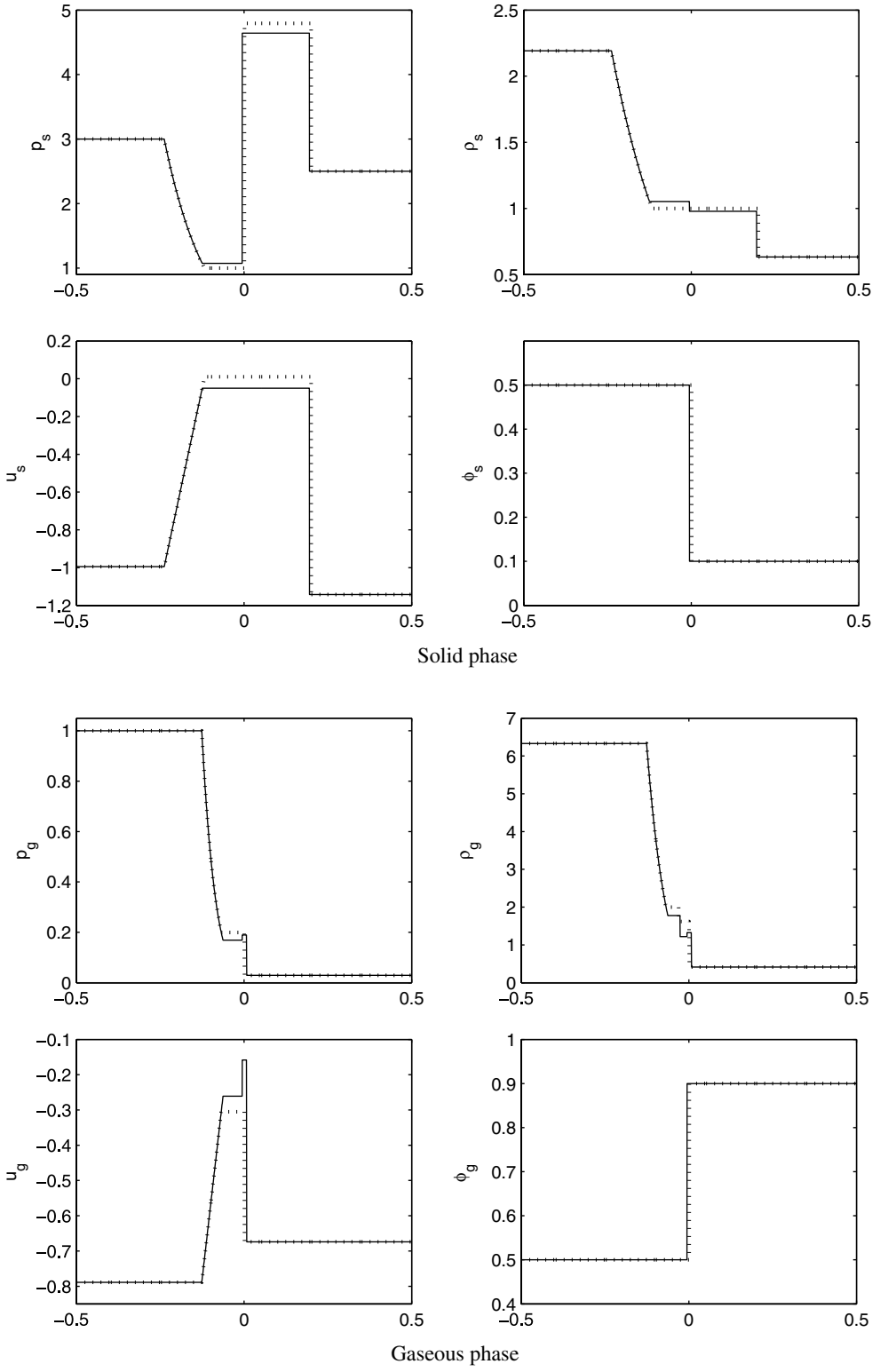

Fig. 11. Two admissible solutions to the Riemann problem with initial states corresponding to the ones of TEST 4 in [13].

dispersive regularization of the system. As a consequence of this regularization, the set of governing equations becomes a non-hyperbolic system. Other types of dispersive regularization (terms responsible for mixture inertia) have been proposed in [16].

(ii) Two-phase flows are essentially multi-dimensional and, therefore, representing them with one-dimensional systems is of very limited use. If this turns out to be true, as in the case of duct flow [13], then the derivation of numerical schemes becomes even more challenging because insofar all such schemes rely on 1D Riemann solvers.

(iii) The form of the volume fraction Eq. (1g) essentially implies that the gas–solid interface moves at the solid phase speed. This might be incorrect. There exist hyperbolic models who assume a different interfacial velocity, for example Saurel and Abgrall [5]. A detailed mathematical analysis of these models is presently lacking. However, it is expected that physically plausible interfacial velocities would still result in linear degeneracy of the corresponding characteristic field.

Finally, it is important to mention that the ill-posedness of the Riemann problem is not of theoretical but of computational interest also. Indeed, even if we try to solve numerically an initial value problem that admits an unique solution, the simulation might stop because a local Riemann problem on a cell interface does not admit a solution. This can be caused by round-off errors or numerical diffusion that change slightly the initial conditions in a way that none of the wave configurations can produce an admissible solution.

8. Conclusions

In this article, a new numerical procedure for solving exactly the Riemann problem of compressible two-phase flow models with non-conservative products has been proposed. In general, the solution of this Riemann problem consists of six distinct non-linear waves: shocks, rarefactions and contact discontinuities. The ordering of these waves in the x–t plane can be classified into four principal families of configurations. Any of these configurations can yield an entropy satisfying solution if certain admissibility criteria are met. The proposed solver examines sequentially the admissibility of these configurations and calculates the solution to the Riemann problem through iterative procedures. Special configurations, corresponding to coalescence of waves, are also included in the solver.

A particularly challenging part in the design of algorithms for the numerical treatment of the governing equations is the accurate integration of the non-conservative products. Three existing methods that perform this were compared through a series of numerical tests. It was predicted that in most circumstances all three methods yield good results. In some cases, however, for example when the jump of the volume fraction across the solid contact is strong, spurious oscillations can arise. These oscillations propagate in the computational domain and their amplitude does not diminish with grid refinement. Our tests indicated that the first and third method produce smaller artificial oscillations than the ones produced by the second method.

Finally, the issue of ill-posedness of the Riemann problem was illustrated through some simple numerical experiments. In particular, it was shown that, depending on the initial conditions, the Riemann problem might possess two solutions or no solution at all. In our view, this phenomenon indicates a breakdown of the validity of the flow models which, therefore, necessitates a revision of the basic assumptions upon which these models have been derived.

References

[1] D.A. Drew, S.L. Passman, Theory of Multicomponent Fluids, Springer, New York, 1998.
[2] H. Enwald, E. Peirano, A.E. Almstedt, Eulerian two-phase flow theory applied to fluidization, Int. J. Multiphase Flow 222 (1986) 21–66.
[3] M.R. Baer, J.W. Nunziato, A two-phase mixture theory for the deflagration-to-detonation transition in reactive granular materials, Int. J. Multiphase Flow 12 (1986) 861–889.
[4] J.M. Powers, D.S. Stewart, H. Krier, Theory of two-phase detonation – part II: structure, Combust. Flame 80 (1990) 280–303.
[5] R. Saurel, R. Abgrall, A multiphase Godunov method for compressible multifluid and multiphase flows, J. Comp. Phys. 150 (1999) 425–467.
[6] J.B. Bdzil, R. Menikoff, S.F. Son, A.K. Kapila, D.S. Stewart, Two-phase modelling of deflagration-to-detonation transition in granular materials: a critical examination of modelling issues, Phys. Fluids 11 (1999) 378–402.

[7] M.V. Papalexandris, A two-phase model for compressible granular flows based on the theory of irreversible processes, J. Fluid Mech. 517 (2004) 103–112.
[8] K.A. Gonthier, J.M. Powers, A high-resolution numerical method for a two-phase model of deflagration-to-detonation transition, J. Comput. Phys. 163 (2000) 376–433.
[9] M.V. Papalexandris, Numerical simulations of detonations in mixtures of gases and solid particles, J. Fluid Mech. 507 (2004) 95–142.
[10] G. Dal Maso, P.G. Lefloch, F. Murat, Definition and weak stability of nonconservative products, J. Math. Pures Appl. 74 (1995) 483–548.
[11] P.G. Lefloch, A.E. Tzavaras, Representation of weak limits and definition of nonconservative products, SIAM J. Math. Anal. 30 (1999) 1309–1342.
[12] G. Crasta, P.G. Lefloch, Existence result for a class of nonconservative and nonstrictly hyperbolic systems, Commun. Pure Appl. Anal. 1 (2002) 1–18.
[13] N. Andrianov, G. Warnecke, The Riemann problem for the Baer-Nunziato two-phase flow model, J. Comput. Phys. 195 (2004) 434–464.
[14] P. Embid, M. Baer, Mathematical analysis of a two-phase continuum mixture theory, Continuum Mech. Thermodyn. 4 (1992) 279–312.
[15] R. Saurel, O. Lemetayer, A multiphase model for compressible flows with interfaces, shocks, detonation waves and cavitation, J. Fluid Mech. 431 (2001) 239–271.
[16] S. Gavrilyuk, R. Saurel, A compressible multiphase model with microinertia, J. Comput. Phys. 175 (2002) 326–360.
[17] R. Abgrall, How to prevent pressure oscillations in multicomponent flow calculations: a quasi conservative approach, J. Comput. Phys. 125 (1996) 150–160.
[18] D.W. Schwendeman, C.W. Wahle, A.K. Kapila, The Riemann problem and a high-resolution Godunov method for a model of compressible two-phase flow, J. Comput. Phys. 212 (2006) 490–526.
[19] P.D. Lax, Hyperbolic systems of conservation laws II, Commun. Pure Appl. Math. 10 (1957) 537–567.
[20] B.L. Keyfitz, H.C. Kranzer, A system of non-strictly hyperbolic conservation laws arising in elasticity theory, Arch. Rat. Mech. Anal. 72 (1980) 219–241.
[21] B.L. Keyfitz, H.C. Kranzer, The Riemann problem for a class of hyperbolic conservation laws exhibiting a parabolic degeneracy, J. Differ. Equations 72 (1983) 35–65.
[22] D.G. Schaeffer, M. Shearer, The classification of 2×2 systems of non-strictly hyperbolic conservation laws with applications to oil recovery, Commun. Pure Appl. Math. 40 (1987) 141–178.
[23] E. Isaacson, B. Temple, Nonlinear resonance in systems of conservation laws, SIAM J. Appl. Math. 52 (1992) 1260–1278.
[24] P. Colella, H.M. Glaz, Efficient solution algorithms for the Riemann problem for real gases, J. Comput. Phys. 59 (1985) 264–289.
[25] B. Fryxell, K. Olson, P. Ricker, F.X. Timmes, M. Zingale, D.Q. Lamb, P. MacNeice, R. Rosner, J.W. Truran, H. Tufo, FLASH: an adaptive-mesh hydrodynamics code for modelling astrophysical thermonuclear flashes, Astroph. J. Supp. Series 131 (2000) 273–334.
[26] B. Braconnier, Université Bordeaux, Private communication, 2005.
[27] B. van Leer, Towards the ultimate conservative difference scheme. V. A second-order sequel to Godunov's method, J. Comput. Phys. 32 (1979) 101–136.
[28] P.G. Lefloch, M.D. Thanh, The Riemann problem for fluid flows in a nozzle with discontinuous cross-section, Commun. Math. Sci. 1 (2003) 763–796.
[29] N. Andrianov, Performance of numerical methods on the non-unique solution to the Riemann problem for the shallow water equations, Int. J. Numer. Meth. Fluids 47 (2005) 825–831.
[30] C. Dafermos, The entropy rate admissibility criterion for solutions of hyperbolic conservations laws, J. Differ. Equations 14 (1973) 202–212.